THE UNIVERSITY OF EDINBURGH

MSc IN THEORETICAL PHYSICS

Multimodal Spin Based Sensors

Conner J ADLINGTON

Supervisor: Professor Cristian Bonato

August 23, 2024

Abstract

Lorem ipsum dolor sit amet, consectetuer adipiscing elit. Ut purus elit, vestibulum ut, placerat ac, adipiscing vitae, felis. Curabitur dictum gravida mauris. Nam arcu libero, nonummy eget, consectetuer id, vulputate a, magna. Donec vehicula augue eu neque. Pellentesque habitant morbi tristique senectus et netus et malesuada fames ac turpis egestas. Mauris ut leo. Cras viverra metus rhoncus sem. Nulla et lectus vestibulum urna fringilla ultrices. Phasellus eu tellus sit amet tortor gravida placerat. Integer sapien est, iaculis in, pretium quis, viverra ac, nunc. Praesent eget sem vel leo ultrices bibendum. Aenean faucibus. Morbi dolor nulla, malesuada eu, pulvinar at, mollis ac, nulla. Curabitur auctor semper nulla. Donec varius orci eget risus. Duis nibh mi, congue eu, accumsan eleifend, sagittis quis, diam. Duis eget orci sit amet orci dignissim rutrum.

Declaration

I declare that this dissertation was composed entirely by myself. Lorem ipsum dolor sit amet, consectetuer adipiscing elit. Ut purus elit, vestibulum ut, placerat ac, adipiscing vitae, felis. Curabitur dictum gravida mauris. Nam arcu libero, nonummy eget, consectetuer id, vulputate a, magna. Donec vehicula augue eu neque. Pellentesque habitant morbi tristique senectus et netus et malesuada fames ac turpis egestas. Mauris ut leo. Cras viverra metus rhoncus sem. Nulla et lectus vestibulum urna fringilla ultrices. Phasellus eu tellus sit amet tortor gravida placerat. Integer sapien est, iaculis in, pretium quis, viverra ac, nunc. Praesent eget sem vel leo ultrices bibendum. Aenean faucibus. Morbi dolor nulla, malesuada eu, pulvinar at, mollis ac, nulla. Curabitur auctor semper nulla. Donec varius orci eget risus. Duis nibh mi, congue eu, accumsan eleifend, sagittis quis, diam. Duis eget orci sit amet orci dignissim rutrum.

Need to write a declaration

Personal Statement

The project began with developing a deeper understanding of the physics underlying spintronics. The main focus was on electron paramagnetic resonance, specifically using the continuous wave optically detected magnetic resonance technique. For this, there is a wealth of literature on the diamond nitrogen vacancy (DNV). Most popular is the application of the DNV as a very sensitive magnetometer.

orked to
derstand
e intricate
tails with
ference to
amond hop-
g I could
ply this
owledge
SiC

I worked to ...

When I felt comfortable with the underlying physics, I began modelling the different system Hamiltonians. I applied varying $\vec{B}$ and $\vec{E}$ as well as varied temperature. The goal was both to understand the influence of these external factors on the spin-system energy levels as well as to verify my model behaved correctly in the simple cases when compared to existing literature.

When I had the capability to dynamically model both the DNV and several SiC defects, with different spin numbers, I created ensembles of specifically chosen defects to visualise how the CW-ODMR spectra might change under the influence of varying $\vec{B}$, $\vec{E}$ and T. This, as well as existing literature allowed me to isolate specific defects which were most appropriate for the sensing of specific variables. For example, the V2 Silicon defect in SiC is very insensitive to changes in temperature so would not be the most appropriate for thermometry application.

When an ensemble of defects was selected for a specific multi-modal application and the nature of the changes to the ODMR spectra was understood, I worked to develop a method to extract and disentangle the influence of each individual influence on the spectra.

This process was repeated for several model systems and in the end I developed a theoretical framework for a multi-modal sensing application of specifically chosen defects in SiC.

During the course of the project, I met with my supervisor every week, in order to discuss my progress and the direction I would head next. Toward the end, the frequency of our meetings increased somewhat, as I began to finish my calculations.

I started writing this dissertation in mid-July, and I spent the first three weeks of August working on it full-time.

Overall, I feel that the project was a success, and I found it to be extremely enjoyable throughout.

Review before submission

Acknowledgements

I'd like to thank my supervisor **Professor Cristian Bonato** for making this project possible, I am particularly grateful for his patience and his ability to make complex subjects seem approachable and achievable.

I would also like to thank the Royal Air Force **Director of Defence Studies** and the **Chief of the Air Staff** for supporting my completion of this research and I look forward to applying what I have learned to my time in service.

Most of all I would like to thank my wife **Sophie** for her ongoing support and patience. I could not have completed this work without your help.

Todo list

Contents

List of Figures

Chapter 1

Introduction

Select clearpage or cleardoublepage depending on contents length

Solid-state colour centres, which exists in many materials such as diamond and silicon carbide, have been one of the leading systems in quantum technology [3, 4]. The nitrogen-vacancy (NV) centre in diamond is the most comprehensively studied solid-state spin defect. The defect spin state can be initialized by laser and controlled by microwave [5, 6, 7]. It has been used in various quantum technologies, such spin–photon entanglement, a quantum computing qubit register and high-sensitivity nanoscale quantum sensing, the focus of this work [8, 9].

The NV centre is favoured for it's for its excellent quantum properties, but drawbacks of the system are a lack of established nanotechnology and the fluorescence wavelength of the NV centre, which is in the visible range and limits its wider applications [10, 11, 12]

The field of spectroscopy studies the way atoms and molecules interact with and exchange energy with a wider physical system - specifically through electromagnetic radiation. The electric field interacts with with the electric dipole moment and the magnetic field interacts with a magnetic dipole moment. Magnetic resonance spectroscopy focusses specifically on the interaction between the $\vec{B}$ field with magnetic moments which exist in a given material. This can be broken into two distinct fields:

Nuclear Magnetic Resonance (NMR) which studies the interaction with nuclear magnetic moments.

Electron Paramagnetic Resonance (EPR) which studies the interaction with magnetic moments of electrons.

Using Planck's relationship $E = h\nu$ and $c = \lambda\nu$ we may characterise the electromagnetic radiation by its energy which is, to a constant, equivalent to the frequency or the wavelength. EPR is observed in systems where the magnetic dipole of the electron is influenced by an applied, oscillating magnetic field forcing transitions between electron energy levels. In general

the measurable difference in energy levels for which the transition occurs is caused by an external magnetic field via the Zeeman effect. Some systems also exhibit energy level splitting in the absence of an applied external magnetic field so called zero field splitting (ZFS).

EPR is thus a tool to manipulate electron spins in solid state materials. The transition between energy levels is quantised thus the discrete amount of energy which is lost by the system is transferred into a photon or charge state which may be detected optically or electrically [13].

A particularly successful technique is Optically Detected Magnetic Resonance (ODMR) which uses an applied microwave frequency, an oscillating magnetic field with energy quanta equivalent to the transitions between Zeeman sub levels, to drive the repopulation of those Zeeman sub levels following a spin-dependent optical transition. In essence this boosts the sensitivity since the microwave driven repopulation induces a change in photoluminescence with a much higher and thus much more readily detectable energy. The techniques of ODMR are so effective that even a single electron spin may be detected this way [14].

Spintronics, a portmantau of **spin** and elec**tronics** is a technology which exploits the characteristics of spin akin to how charge is manipulated in electronics. Fundamentally, the smallest stable magnetic moment available in nature is generated by the spin of a single electron. If efficient read-out can be achieved, the sensitivity of the electron magnetic dipole cannot be matched. Careful construction of an appropriate system, or identification of a system with appropriate characteristics allows for the initialisation, manipulation and read-out of EPR from which we may infer the physical properties of the environment surrounding the system.

With ODMR of the NV centre in diamond the manipulation of spin states in single, atomic-sized centres at room temperature has been demonstrated [15] despite spin polarisation being a primarily thermodynamic effect (see section **??**). This is possible since optical excitation of the energy levels decay faster via a spin-preserving transition, leading to an inverse population of spin sublevels in its ground state when the system is irradiated consistently for several excitation/decay cycles.

This prompted the search for other structures with similar unique quantum properties. Silicon carbide (SiC) is a promising candidate (discussed in detail in section **??**). A major benefit of SiC is the existence of various polytypes, which each exhibit unique spin colour centre properties. Furthermore, even within a single polytype, these centres can occupy distinct and non-equivalent lattice positions. The existence of these colour centres with similar properties but different energy quanta allows for selection of a specific defect with parameters suitable for the problem at hand.

EPR spectroscopy can be approached by different methods, relevant to this work:

Continuous Wave (CW) where the magnitude of the static magnetic field (B_0) is swept, while the amplitude of the driving field B_1 is constant with time.

Electron-Electron Double Resonance (ELDOR) where two microwave frequencies participate;

1. The “pump” microwave source, irradiates a portion of the ESR spectrum.
2. The effect of this irradiation on another portion of the spectrum is monitored by an observe microwave source. [16]

This work looks to explore how the physical characteristics which influence the Spin Hamiltonian and thus the energy of the electron spin system may be inferred by measuring the effects of those characteristics on the EPR of that system. Further, it will look to explore whether the compound effect of multiple influences may be disentangled and measured simultaneously - so called multi-modal sensing.

Write introduction chapter summary

Chapter 2 gives...

In Chapter 3 we...

Then, in Chapter **??** we...

Finally we conclude in Chapter **??**

Chapter 2

Background

2.1 Magnetism

Where charge ($\vec{E}$-field) has an elementary source unit of a point charge (or monopole) which may be positively or negatively charged. Conversely the elementary source unit of magnetism ($\vec{B}$-field) is the magnetic dipole.

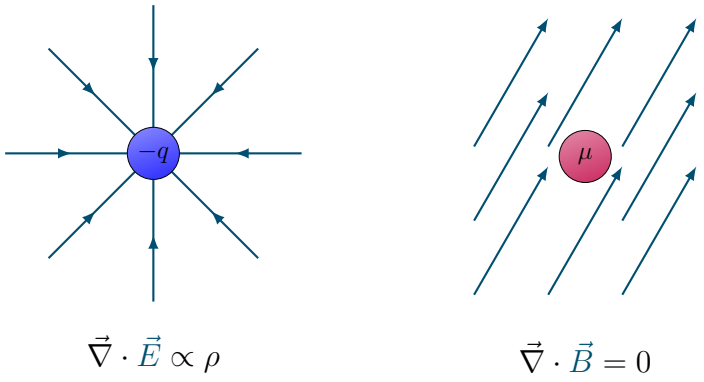

Fig. 2.1: Schematic of electric monopole and magnetic dipole with associated field lines and relevant Maxwell equation.

Magnetic monopoles have never been observed; their existence would also violate Gauss' law ($\vec{\nabla} \cdot \vec{B} = 0$) [17].

2.1.1 Magnetic Dipole

Classically, the magnetic dipole may be modelled as a closed loop that carries an electric current.

Its magnetic dipole moment, $\vec{\mu}$, is defined as the vector which points out of the plane of the

current loop,

$$\vec{\mu} = IS\vec{n} \tag{2.1}$$

where I is the current in, and S the surface area enclosed by, the loop.

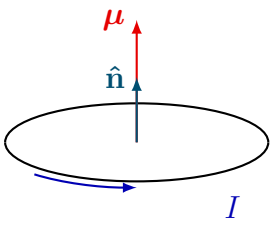

Fig. 2.2: Schematic of current loop and induced magnetic moment.

The magnetic dipole produces a magnetic field $\vec{B}$, which for points a large distance from the dipole may be calculated as [18]:

$$\vec{B} = \frac{\mu_0}{4\pi}\frac{1}{r^3}\left[\frac{3(\vec{\mu}\cdot\vec{r})\cdot\vec{r}}{r^2} - \vec{\mu}\right] \tag{2.2}$$

The symmetry of the field enables us to consider the direction of the dipole as aligned to the z-axis. Then, defining x, y as usual by $r\cos\theta$ and $r\sin\theta$ respectively. We may decompose the magnetic field in two separate components, parallel (B_z) and perpendicular (B_x, B_y):

$$B_{\parallel} = \frac{\mu_0}{r^3}(3\cos^2\theta - 1), \quad B_{\perp} = \frac{3\mu_0}{r^3}\cos\theta\sin\theta.$$

Where we use the Pythagorean principle to determine the overall magnitude $B = |\vec{B}|$ as

$$B = \sqrt{B_{\parallel}^2 + B_{\perp}^2}.$$

2.1.2 Gyromagnetic Ratio

Classical Derivation

The current in (2.1) is proportional to the angular momentum of the charge; that is, the dipole moment is always associated with an angular momentum $\vec{G} = \vec{r}\times\vec{p}$ with $\vec{r}$ the radius and $\vec{p}$ the momentum.

Dividing the magnetic dipole moment by the angular momentum we find the **gyromagnetic ratio** [19]

$$\gamma = \frac{\vec{\mu}}{\vec{G}}. \tag{2.3}$$

Without loss of generality we may consider the most simple case, in which the magnetic dipole moment is parallel (or anti-parallel) to the angular momentum. Then using the absolute values for the dipole moment and the angular momentum

$$\mu = IS, \quad I = \frac{qv}{2\pi R}, \quad S = \pi R^2 \tag{2.4}$$

we substitute I and S to find

$$\mu = \frac{qvR}{2} \tag{2.5}$$

and further, we equate the angular momentum vector, using the model of a planar loop to

$$G = m_q v R \tag{2.6}$$

leaving

$$\gamma = \frac{q}{2m_q}. \tag{2.7}$$

We finally consider that we may represent the, currently arbitrary, charge and mass as a sum of electron charges and masses.

$$\gamma = \frac{q}{2m_q} = \frac{\cancel{N}e}{2\cancel{N}m_e} \implies \gamma = \frac{e}{2m_e} \tag{2.8}$$

We therefore find that the gyromagnetic ratio of the electron depends only on fundamental constants [20].

Extending to Quantum Mechanics

Since the gyromagnetic ratio was calculated considering the motion of dipole in a loop, we may extend this to an electron in an orbit. The fundamental change required to extend the model to quantum mechanics is the treatment of angular momentum which should now be quantised. Thus, we replace our classical approximation of $\vec{G} = \vec{r} \times \vec{p}$ with the equation for the eigenvalues of the quantum mechanical representation of orbital angular momentum,

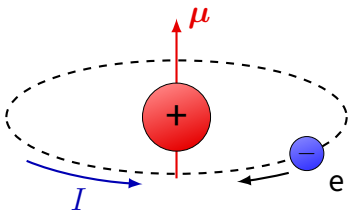

Fig. 2.3: Schematic of electron in orbit generating a magnetic moment.

$$\hat{G} = \hbar \hat{L} \tag{2.9}$$

where $\hat{L}$ is the operator of the orbital angular momentum (quantum number of orbital momentum). The angular momentum and total energy are conserved in general in a closed system.

We consider the time independent Shrödinger equation

$$\hat{H}\Psi_n = E_n \Psi_n \tag{2.10}$$

and choose Ψ_n such that it is an eigenfunction of the Hamiltonian, the total angular momentum squared ($L^2 = L_x^2 + L_y^2 + L_z^2$) and exactly one directional component of the angular momentum which is by convention chosen as L_z.

According to quantum mechanics the projection of L along the (m_L) may take integer values $-L, -L+1, \ldots, L-1, L$. Thus, we may describe a given quantum state by the angular momentum L and it's projection m_L. Thus, using Dirac Notation we write

$$\hat{H}\left|L, m_L\right\rangle = E\left|L, m_L\right\rangle \tag{2.11}$$
$$\hat{L}^2\left|L, m_L\right\rangle = L(L+1)\left|L, M_L\right\rangle \tag{2.12}$$
$$\hat{L}_z\left|L, m_L\right\rangle = m_L\left|L, m_L\right\rangle. \tag{2.13}$$

Thus, the operator which describes the orbital magnetic moment may be written using (2.8), (2.9) as

$$\hat{\vec{\mu}}_L = \gamma\hat{\vec{G}}_L = \gamma\hbar\hat{\vec{L}} = \frac{e\hbar}{2m_e c}\hat{\vec{L}}. \tag{2.14}$$

This leads to a quantity known as the **Bohr Magneton**, μ_B, given by [21]

$$\mu_B = \frac{|e|\hbar}{2m_e c}. \tag{2.15}$$

Using this we may write (2.14) as

$$\hat{\vec{\mu}}_L = -\mu_B\hat{\vec{L}}, \tag{2.16}$$

and we may relate the Bohr magneton and the gyromagnetic ratio for the electron as

$$\gamma = g\mu_B. \tag{2.17}$$

2.1.3 g-factor

The above expression is valid for the orbital electron but may be extended to a more general system by introducing a g-factor. The g-factor is equivalent to a dimensionless gyromagnetic ratio [22], so (2.16) may be written with $g = 1$ as

$$\hat{\vec{\mu}}_L = -g\mu_B\hat{\vec{L}}. \tag{2.18}$$

2.2 Spin

As well as the orbital magnetic moment generated by the orbital angular momentum of the electron, the electron also possesses an intrinsic magnetic moment. Classically this implies an intrinsic angular momentum hence the magnetic moment of elementary particles is termed spin. For a single electron spin may take the value $\pm 1/2$ since the system has only been ob-

served in two possible states [23] and experiments confirm that the orbital angular momentum and spin angular momentum are of the same nature and thus may be summed. The magnetic moment of the spin may thus be expressed as (2.18) [24] where $g \approx 2.0023$ [25, 26].

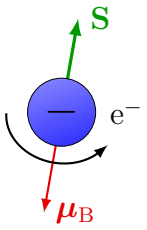

In reality the electron is point-like and thus the current loop model is unsuitable. Spin is actually a purely quantum mechanical effect and a consequence of the algebra required to satisfy the Dirac equation of relativistic quantum mechanics. The manifestation of this degree of freedom however has the same dimensionality as $\vec{L}$, allowing us to work with the combination of $\vec{L}$ and $\vec{S}$.

We thus consider the total angular momentum of a system J given by

$$J = L + S \tag{2.19}$$

which make take the values $L + S, L + S - 1, \ldots, |L - S|$.

For a given system with two electrons, combining the individual spin angular momenta, total spin angular momentum is the addition of the uncoupled spin operators

$$\hat{S} = \hat{S}_1 + \hat{S}_2 \tag{2.20}$$

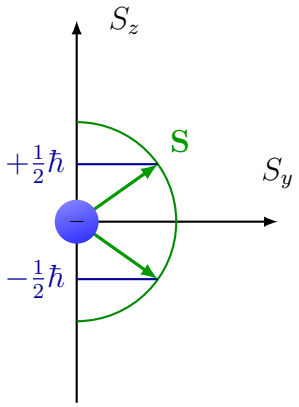

Fig. 2.4: Schematic of discrete spin levels.

The coupling results in the formation of four spin states with spin quantum number $S = 0$ and $S = 1$. The spin quantum number $S = 0$ leads to a multiplicity of $2S + 1 = 1$, a so called singlet state.

However, the spin quantum number $S = 1$ results in a multiplicity of $2S + 1 = 3$, known as triplet states [27].

2.3 Zeeman Effect

When no magnetic field is applied to a system, the magnetic dipoles of the orbital electron and spin have no preferred direction. The energy levels for all combinations of L and S (all J) are equivalent.

If a magnetic field is applied the magnetic moments interact with that field via the Zeeman interaction. The Zeeman effect consists of atomic energy level splitting when an external magnetic field is imposed on a sample [28].

The classical expression for the energy of a dipole in a magnetic field

$$E = -\vec{\mu} \cdot \vec{B} \tag{2.21}$$

may be replaced with the Hamiltonian for a quantum mechanical system

$$\hat{H}_{\text{Zeeman}} = -\hat{\vec{\mu}} \cdot \vec{B}. \tag{2.22}$$

The negative sign indicates that when the magnetic moment is parallel to the magnetic field the lowest energy is achieved.

Thus distinct quantum systems with different J and thus different projections of angular momentum (m_J) have different energies due to their interaction with a magnetic field.

Considering a simple two-level system ($S = 1/2$), the energy difference between the spin being aligned or anti-aligned with the field is called the Zeeman energy.

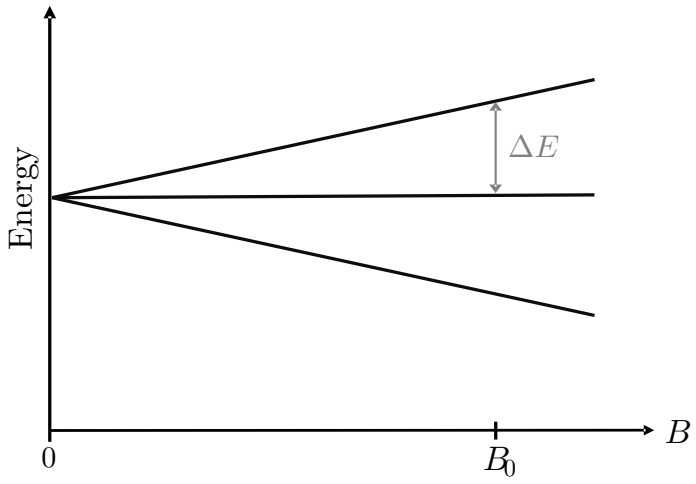

Fig. 2.5: Adapted from figure shown in the work by Grüne.

The Hamiltonian to describe the energy is, using the total angular momentum form of (2.18),

$$\hat{H}_{\text{Zeeman}} = g\mu_B \hat{\vec{S}} \cdot \vec{B}. \tag{2.23}$$

Without loss of generality we may direct the magnetic field along the z axis and reduce the scalar product to only the z component. Now, using $S = 1/2$ quantised along the z axis, i.e. $m_S = \pm 1/2$ we find the Zeeman energy by solving the Shrödinger equation

$$\hat{H}_{\text{Zeeman}} \left|S, m_S\right\rangle = E_{\text{Zeeman}} \left|S, m_S\right\rangle \tag{2.24}$$

which, to a factor is equivalent to, by (2.13), to

$$\hat{S}_z \left|S, m_S\right\rangle = m_S \left|S, m_S\right\rangle . \tag{2.25}$$

Thus we find the two eigenvalues to be

$$E_+ = \frac{1}{2} g\mu_B B, \qquad E_- = -\frac{1}{2} g\mu_B B \tag{2.26}$$

and thus the Zeeman energy is given by $g\mu_B B$.

The $S = 1/2$ system is thus doubly degenerate and the degeneracy is lifted by the application a magnetic field. The Zeeman energy is the difference between the two states and it grows linearly with B.

This may be generalised to a more complex system by considering the total angular momentum J where the energy difference between states is given by

$$\Delta E = g_J \mu_B B. \tag{2.27}$$

2.4 Spin-Orbit Interaction

The orbital magnetic dipole may interact with the intrinsic spin magnetic dipole via the spin-orbit interaction. This is represented by the spin-orbit Hamiltonian with λ representing the constant of the coupling:

$$H_{\mathrm{SO}} = \lambda \hat{\vec{L}} \cdot \hat{\vec{S}}. \tag{2.28}$$

This is caused by the interaction between the magnetic field generated by the relativistic motion of the electron around the nucleus and that of the spin magnetic moment. The coupling is proportional to the atomic mass.

2.5 Perturbation Theory

By considering a ground, non-degenerate state and a perturbation in the electron Zeeman interaction and the spin-orbit coupling we can develop insight into so called zero field splitting. The perturbation is given by

$$\hat{H}' = \hat{H}_{\mathrm{Zeeman}} + \hat{H}_{\mathrm{SO}} \tag{2.29}$$

for which we find

$$E_0 = E_0^{(0)} + \langle 0| \hat{H}' |0\rangle + \sum_n \frac{\langle 0| \hat{H}' |n\rangle \langle n| \hat{H}' |0\rangle}{E_0^{(0)} - E_n^{(0)}}. \tag{2.30}$$

Now, if we consider arbitrary interactions of forms

$$\hat{H}_{\mathrm{Zeeman}} = g_L \mu_B \hat{\vec{L}} \cdot \vec{B} + g_S \mu_B \hat{\vec{S}} \cdot \vec{B} \tag{2.31}$$

$$\hat{H}_{\mathrm{SO}} = \lambda \hat{\vec{L}} \cdot \hat{\vec{S}} \tag{2.32}$$

we may compute the first and second order corrections.

First Order

Substituting (2.31) and (2.32) into (2.30) and integrating only over the orbital values to deduce the Spin Hamiltonian we find

$$\begin{aligned}
\langle 0|\,\hat{H}'\,|0\rangle &= \langle 0|\,g_L\mu_B\hat{\vec{L}}\cdot\vec{B} + g_S\mu_B\hat{\vec{S}}\cdot\vec{B} + \lambda\hat{\vec{L}}\cdot\hat{\vec{S}}\,|0\rangle \\
&= \langle 0|\,g_L\mu_B\hat{\vec{L}}\cdot\vec{B}\,|0\rangle + \langle 0|\,g_S\mu_B\hat{\vec{S}}\cdot\vec{B}\,|0\rangle + \langle 0|\,\lambda\hat{\vec{L}}\cdot\hat{\vec{S}}\,|0\rangle \\
&= g_L\mu_B\vec{B}\cdot\langle 0|\,\hat{\vec{L}}\,|0\rangle + g_S\mu_B\vec{B}\cdot\hat{\vec{S}}\,\langle 0|0\rangle + \lambda\hat{\vec{S}}\cdot\langle 0|\hat{\vec{L}}|0\rangle \\
&= g_L\mu_B\vec{B}\cdot\cancelto{0}{\langle 0|\hat{\vec{L}}\,|0\rangle} + g_S\mu_B\vec{B}\cdot\hat{\vec{S}}\cancelto{1}{\langle 0|0\rangle} + \lambda\hat{\vec{S}}\cdot\cancelto{0}{\langle 0|\hat{\vec{L}}|0\rangle} \\
&= g_s\mu_B\hat{S}\cdot\hat{B}.
\end{aligned} \tag{2.33}$$

Here we used the fact that $\langle 0|\hat{\vec{L}}|0\rangle = 0$ since, for example in the alegbraic basis $\hat{L}_z = -i\left(x\frac{\partial}{\partial y} - y\frac{\partial}{\partial x}\right)$ is a Hermitian operator is therefore has eigenvalues which are strictly real numbers, i.e.

$$\hat{L}_z\,|\psi\rangle = m_L\,|\psi\rangle\,. \tag{2.34}$$

By considering (2.34) we see that if we apply an imaginary operator to a real valued eigenfunction the corresponding eigenvalue must be imaginary or zero. We know the state is strictly real since it is non-degenerate[1]. In this case, the expectation value of $\hat{L}$ can only be 0.

Zeeman Splitting. The result of the first order perturbation is thus a more formal confirmation of the result of section 2.3, specifically (2.27).

Second Order

At second order, again substituting (2.31) and (2.32) into (2.30) and integrating only over the orbital values we find

$$\sum_n \frac{\langle 0|\,\hat{H}'\,|n\rangle\,\langle n|\,\hat{H}'\,|0\rangle}{E_0^{(0)} - E_n^{(0)}}$$

[1] A complex wavefunction ψ is at least doubly degenerate; the complex conjugate ψ^* has the same energy.

$$
\begin{aligned}
&= \frac{\langle 0|g_L\mu_B\hat{\vec{L}}\cdot\vec{B}+g_S\mu_B\hat{\vec{S}}\cdot\vec{B}+\lambda\hat{\vec{L}}\cdot\hat{\vec{S}}|n\rangle\langle n|g_L\mu_B\hat{\vec{L}}\cdot\vec{B}+g_S\mu_B\hat{\vec{S}}\cdot\vec{B}+\lambda\hat{\vec{L}}\cdot\hat{\vec{S}}|0\rangle}{E_0^{(0)}-E_n^{(0)}} \\
&= \frac{\langle 0|g_L\mu_B\hat{\vec{L}}\cdot\vec{B}+\lambda\hat{\vec{L}}\cdot\hat{\vec{S}}|n\rangle\langle n|g_L\mu_B\hat{\vec{L}}\cdot\vec{B}+\lambda\hat{\vec{L}}\cdot\hat{\vec{S}}|0\rangle}{E_0^{(0)}-E_n^{(0)}} \\
&= (g_L\mu_B\vec{B}+\lambda\hat{\vec{S}})\underbrace{\sum_n\frac{\langle 0|\hat{\vec{L}}|n\rangle\langle n|\hat{\vec{L}}|0\rangle}{E_0^{(0)}-E_n^{(0)}}}_{\Lambda}(g_L\mu_B\vec{B}+\lambda\hat{\vec{S}})
\end{aligned}
\tag{2.35}
$$

Here Λ is a matrix composed of the elements as shown. Expanding out, this allows us to write the second order perturbation as

$$
\sum_n\frac{\langle 0|\hat{H}'|n\rangle\langle n|\hat{H}'|0\rangle}{E_0^{(0)}-E_n^{(0)}} = g_L^2\mu_B^2\vec{B}\cdot\Lambda\cdot\vec{B}+2\lambda g_L\mu_B\hat{\vec{S}}\cdot\Lambda\cdot\vec{B}+\lambda^2\hat{\vec{S}}\cdot\Lambda\cdot\hat{\vec{S}}. \tag{2.36}
$$

Since for EPR we are only interested in the spin-dependent terms, the first term may be neglected as it represents a global shift in the energy spectra.

Combined Perturbation

Combining (2.33) and (2.36) we find

$$
\begin{aligned}
\langle 0|\hat{H}'|0\rangle+\sum_n\frac{\langle 0|\hat{H}'|n\rangle\langle n|\hat{H}'|0\rangle}{E_0^{(0)}-E_n^{(0)}} &= g_S\mu_B\hat{\vec{S}}\cdot\vec{B}+2\lambda g_L\mu_B\hat{\vec{S}}\cdot\Lambda\cdot\vec{B}+\lambda^2\hat{\vec{S}}\cdot\Lambda\cdot\hat{\vec{S}} \\
&= \mu_B\hat{\vec{S}}\cdot\underbrace{(g_S+2g_L\lambda\Lambda)}_{g}\cdot\vec{B}+\hat{\vec{S}}\cdot\underbrace{\lambda^2\Lambda}_{D}\cdot\hat{\vec{S}}.
\end{aligned}
\tag{2.37}
$$

In this expression g and D are matrix quantities depending on Λ and represent the (possibly anisotropic) g factor and D the fine structure splitting.

For this work we will consider only systems in which the differences in angular momentum is due only to the spin and thus g is reduced to a scalar quantity in the spin Hamiltonian.

write captio

The term depending on D has no dependence on magnetic field and thus this fine-structure splitting is known as zero field splitting (ZFS) and is observed in systems with $S > 1/2$.

$$
H_{\mathrm{FS}} = \hat{\vec{S}}\cdot D\cdot\hat{\vec{S}}. \tag{2.38}
$$

2.6 Zero Field Splitting

ZFS is in fact due to the combined effects of fine structure and a dipole-dipole interaction. These

effects manifest themselves identically which makes them difficult to separate experimentally. They each depend on a traceless matrix D, as will be shown, which can be totally described by two parameters, conventionally labelled D and E. For simplicity in this work we will consider the combined effect of both the fine-structure and the dipole-dipole interaction as the ZFS interaction. This means when D and E are measured for a specific system, they represent the compound effect of fine-structure splitting and the dipole interaction, but totally describe the zero-field splitting.

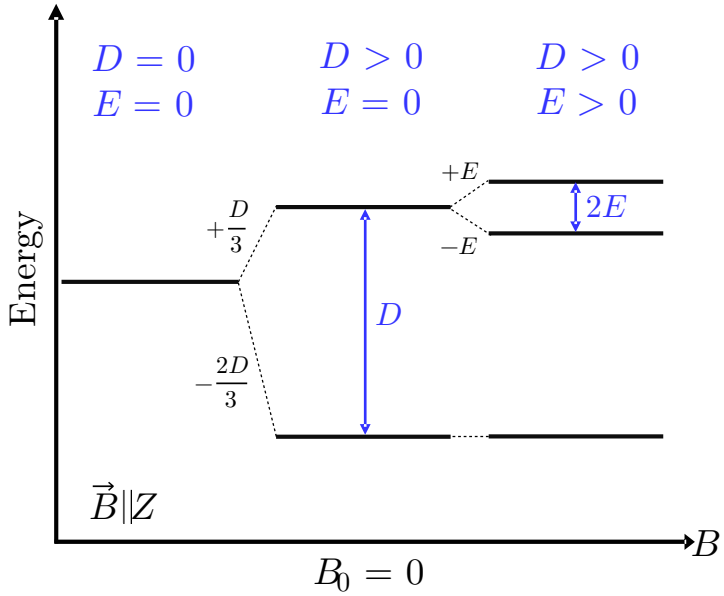

Fig. 2.6: Adapted from figure shown in the work by Grüne.

2.6.1 Fine Structure

The matrix D in (2.38) has form

$$D = \begin{pmatrix} D_{xx} & D_{xy} & D_{xz} \\ D_{yx} & D_{yy} & D_{yz} \\ D_{zx} & D_{zy} & D_{zz} \end{pmatrix} \tag{2.39}$$

which may be simplified by alignment to the wider system axis and diagonalising the matrix as

$$D = \begin{pmatrix} D_{xx} & 0 & 0 \\ 0 & D_{yy} & 0 \\ 0 & 0 & D_{zz} \end{pmatrix}. \tag{2.40}$$

The trace of the matrix $\mathrm{Tr}(D)$ is unchanged by the change of basis. Since for EPR we are only

concerned with the changes in energy and not the absolute, we may choose the value of the trace without any loss of generality, so we set it equal to zero.

$$\mathrm{Tr}(D) = 0. \tag{2.41}$$

This means that the diagonal form of D may be fully determined by just two parameters

$$D = D_{zz} - (D_{xx} + D_{yy})/2 \tag{2.42}$$
$$E = (D_{xx} - D_{yy})/2 \tag{2.43}$$

Here D represents the axially symmetric parameter and E represents any non-axial contribution of the fine-structure interaction.

Substituting (2.42) and (2.43) into (2.38) and expanding allows us to write our fine-structure Hamiltonian as

$$H_{\mathrm{FS}} = D\left(\hat{S}_z^2 - \frac{1}{3}S(S+1)\right) + E\left(\hat{S}_x^2 - \hat{S}_y^2\right). \tag{2.44}$$

2.6.2 Dipole-Dipole Interaction

We will now show that the interaction between the magnetic dipoles of two electrons has the same form as (2.38) by considering two electrons ($S = 1/2$).

We begin with the classical expression for the energy between two magnetic dipoles, μ_1, μ_2

$$E = \frac{1}{r^3}\left(\mu_1 \cdot \mu_2 - \frac{3(\mu_1 \cdot \vec{r})(\mu_2 \cdot \vec{r})}{r^2}\right). \tag{2.45}$$

Substituting the quantum mechanical operators for the two electron magnetic dipoles we find

$$H_{\mathrm{DD}} = g_S^2 \mu_B^2 \frac{1}{r^3}\left(\hat{\vec{S}}_1 \cdot \hat{\vec{S}}_2 - \frac{3(\hat{\vec{S}}_1 \cdot \vec{r})(\hat{\vec{S}}_2 \cdot \vec{r})}{r^2}\right). \tag{2.46}$$

Considering the total spin of the system we may expand this to obtain [13]

$$H_{\mathrm{DD}} = \frac{1}{2r^5} g_S^2 \mu_B^2 \hat{\vec{S}} \cdot \underbrace{\begin{pmatrix} r^2 - 3x^2 & -3xy & -3xz \\ -3xy & r^2 - 3y^2 & -3yz \\ -3xz & -3yz & r^2 - 3z^2 \end{pmatrix}}_{D} \cdot \hat{\vec{S}}. \tag{2.47}$$

As with (2.40) the matrix D in (2.47) has a constant trace (which we may select to be 0) leaving the form of the dipole-dipole interaction identical to that of the fine structure interaction

$$H_{\mathrm{DD}} = \hat{\vec{S}} \cdot D \cdot \hat{\vec{S}}. \tag{2.48}$$

We therefore decompose the traceless matrix D into the axial and non-axial parameters D and E as above.

2.6.3 Zero Field Splitting Hamiltonian

When measuring the values of D and E experimentally, the combined effect will be contained within those measurements so we may therefore describe the zero field splitting interaction as a whole using

$$H_{\mathrm{ZFS}} = D\left(\hat{S}_z^2 - \frac{1}{3}S(S+1)\right) + E\left(\hat{S}_x^2 - \hat{S}_y^2\right). \tag{2.49}$$

The effects of D and E on a triplet state are illustrated in Figure 2.6.

2.7 Nuclear Hamiltonians

There are three additional contributions to the Hamiltonian to be considered which involve an interaction with the nucleus.

2.7.1 Nuclear Zeeman

Equivalent to electron Zeeman interaction but for the nuclear magnetic moment.

$$H_{\mathrm{Zeeman\,(n)}} = -g_n \mu_n \vec{B} \cdot \hat{\vec{I}} \tag{2.50}$$

It is clear that this contribution is not spin-dependent, therefore it will manifest as a global energy shift and is not of interest for EPR. For this reason, the nuclear Zeeman interaction contribution will not be included for the remainder of this work.

2.7.2 Nuclear Quadrupole

Equivalent to the electron dipole-dipole but for nuclear magnetic moments.

$$H_{\mathrm{Quadrupole}} = \hat{\vec{I}} \cdot Q \cdot \hat{\vec{I}} \tag{2.51}$$

As for the nuclear Zeeman interaction, this contribution is not spin-dependent and the contribution will not be included for the remainder of this work.

2.7.3 Hyperfine Interaction

Equivalent to Fine Structure (ZFS) but between the nuclear and electron moment.

$$H_{\text{Hyperfine}} = \hat{\vec{S}} \cdot A \cdot \hat{\vec{I}} \tag{2.52}$$

$$H_{\text{Hyperfine}} = A_{\parallel} \hat{S}_z \hat{I}_z + A_{\perp} (\hat{S}_y \hat{I}_y + \hat{S}_z \hat{I}_z) \tag{2.53}$$

For the systems discussed in this work, hyperfine couplings are usually too small to detect, thus manifest as inhomogeneous line broadening [29]. We therefore do not include the hyperfine contribution for the remainder of this work.

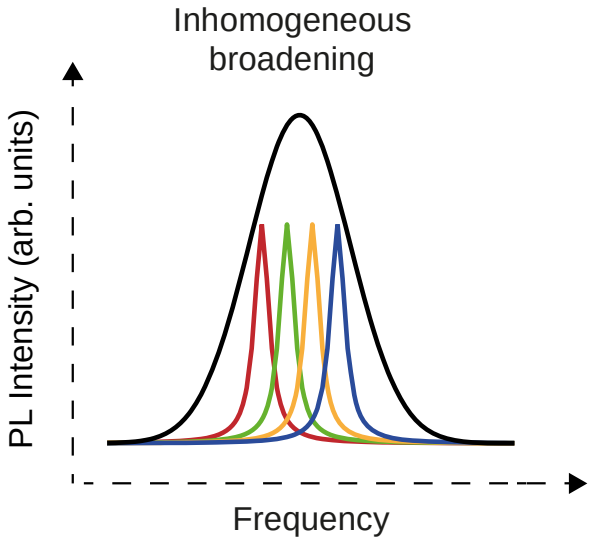

Fig. 2.7: Illustration of the inhomogeneous line broadening caused by the hyperfine interactions. The individual resonances sum to a broader, brighter peak [2].

2.8 Stark Effect

For our Spin Hamiltonian given by

$$\begin{aligned} H &= H_{\text{ZFS}} + H_{\text{Zeeman}} + H_{\text{Hyperfine}} + H_{\text{Zeeman (n)}} + H_{\text{Quadrupole}} \\ H &= \hat{\vec{S}} \cdot \vec{D} \cdot \vec{S} + g\mu_b \hat{\vec{S}} \cdot \vec{B} + \hat{\vec{S}} \cdot A \cdot \hat{\vec{I}} - \mu_n g_n \hat{\vec{I}} \cdot \vec{B} + \hat{\vec{I}} \cdot Q \cdot \hat{\vec{I}}. \end{aligned} \tag{2.54}$$

In the most general sense, an applied electrical field could change any of the parameters. We will not consider the effect of an applied electrical field on the nuclear Zeeman term as the nuclear is paramagnetically shielded [30]. Thus, in a general sense we may add the contributions of an

applied electrical field $\vec{E}$ as $H + H_{\text{Stark}}$ where

$$H_{\text{Stark}} = \vec{E} \cdot \left(\hat{\vec{S}} \cdot R \cdot \hat{\vec{S}} + T\mu_B \hat{\vec{S}} \cdot \vec{B} + \hat{\vec{S}} \cdot F \cdot \hat{\vec{I}} + \hat{\vec{I}} \cdot q \cdot \hat{\vec{I}} \right). \tag{2.55}$$

Here R, T, F, q are matrices for each component of the electric field given by

$$R_{ijk} = \frac{\partial D_{jk}}{\partial E_i}, \quad T_{ijk} = \frac{\partial g_{jk}}{\partial E_i}, \quad F_{ijk} = \frac{\partial A_{jk}}{\partial E_i}, \quad q_{ijk} = \frac{\partial Q_{jk}}{\partial E_i}. \tag{2.56}$$

We may immediately simplify T as for this work we assume isotropic and constant g, for which T is zero.

Further, as discussed in section 2.7 we will not include the contributions of the nuclear Hamiltonians.

This allows us to then consider only the energy change due to the shift in the D parameter, that is R, which is a square matrix for each component of the applied $\vec{E}$. Exactly as we did for ZFS in section 2.6, we may reduce each of these symmetric matrices to a traceless form.

Consider the expansion of $\hat{\vec{S}} \cdot R \cdot \hat{\vec{S}}$ which we calculate explicitly

$$\begin{aligned} \hat{\vec{S}} \cdot R \cdot \hat{\vec{S}} &= \begin{pmatrix} \hat{S}_x & \hat{S}_y & \hat{S}_z \end{pmatrix} \cdot \begin{pmatrix} R_{xx} & R_{xy} & R_{xz} \\ R_{xy} & R_{yy} & R_{yz} \\ R_{xz} & R_{yz} & R_{zz} \end{pmatrix} \cdot \begin{pmatrix} \hat{S}_x \\ \hat{S}_y \\ \hat{S}_z \end{pmatrix} \\ &= R_{xx}\hat{S}_x^2 + R_{yy}\hat{S}_y^2 + R_{zz}\hat{S}_z^2 \\ &+ R_{xy}(\hat{S}_x\hat{S}_y + \hat{S}_y\hat{S}_x) + R_{xz}(\hat{S}_x\hat{S}_z + \hat{S}_z\hat{S}_x) + R_{yz}(\hat{S}_y\hat{S}_z + \hat{S}_z\hat{S}_y). \end{aligned} \tag{2.57}$$

We set the constant trace equal to zero and rewrite

$$R_{xx}\hat{S}_x^2 + R_{yy}\hat{S}_y^2 + R_{zz}\hat{S}_z^2 = R_D \left(\hat{S}_z^2 - \frac{1}{3}S(S+1) \right) + R_E \left(\hat{S}_x^2 - \hat{S}_y^2 \right). \tag{2.58}$$

Where R_D and R_E are defined in terms of R the same way D and E are in terms of D, see (2.42), (2.43).

Then, we may write H_{Stark} in this basis as

$$\begin{aligned} H_{\text{Stark}} = \vec{E} \cdot \Bigg(& R_D \left(\hat{S}_z^2 - \frac{1}{3}S(S+1) \right) + R_E \left(\hat{S}_x^2 - \hat{S}_y^2 \right) \\ & + R_{xy}(\hat{S}_x\hat{S}_y + \hat{S}_y\hat{S}_x) + R_{xz}(\hat{S}_x\hat{S}_z + \hat{S}_z\hat{S}_x) + R_{yz}(\hat{S}_y\hat{S}_z + \hat{S}_z\hat{S}_y) \Bigg). \end{aligned} \tag{2.59}$$

The final step is to reduce the number of coefficients by exploiting the symmetry of the system. We will study systems with the point group symmetry of C_{3v} [31] which reduces the Hamiltonian

again to [30]

$$\begin{aligned} H_{\text{Stark}} = R_{113}\left(E_x(\hat{S}_x\hat{S}_y + \hat{S}_z\hat{S}_x) + E_y(\hat{S}_y\hat{S}_z + \hat{S}_z\hat{S}_y)\right) \\ - R_{2E}\left(E_x(\hat{S}_x\hat{S}_y + \hat{S}_y\hat{S}_x) + E_y(\hat{S}_x^2 - \hat{S}_y^2)\right) \\ + R_{3D}E_z\left(\hat{S}_z^2 - \frac{1}{3}S(S+1)\right) \end{aligned} \tag{2.60}$$

The coefficient R_{113} represents a mixing of the $m_S = 0$ and $m_S = \pm 1$ states which have an energy splitting of $\mathcal{O}(10^9)$ Hz. The Stark energies are $\sim \mathcal{O}(10^3)$ Hz and of at least second order, thus may be ignored [32].

Thus finally, we write our Stark Hamiltonian as

$$H_{\text{Stark}} = d_{\parallel}E_z\left(\hat{S}_z^2 - \frac{1}{3}S(S+1)\right) - d_{\perp}E_y(\hat{S}_x^2 - \hat{S}_y^2) + d_{\perp}E_x(\hat{S}_x\hat{S}_y + \hat{S}_y\hat{S}_x) \tag{2.61}$$

where we have labelled the axial contribution as $d_{\parallel}$ and the off-axis contribution as $d_{\perp}$ to match the convention of existing literature.

By direct comparison to (2.49) it is easy to see the first two terms of (2.61) will contribute to the effective ZFS.

In general longitudinal fields along the defect's symmetry axis result in equal shifts of all levels, whereas transverse fields split the orbitals into two branches whose energy difference grows with increasing field [33, 34]. This allows the parameters $d_{\perp}$ and $d_{\parallel}$ to be measured experimentally.

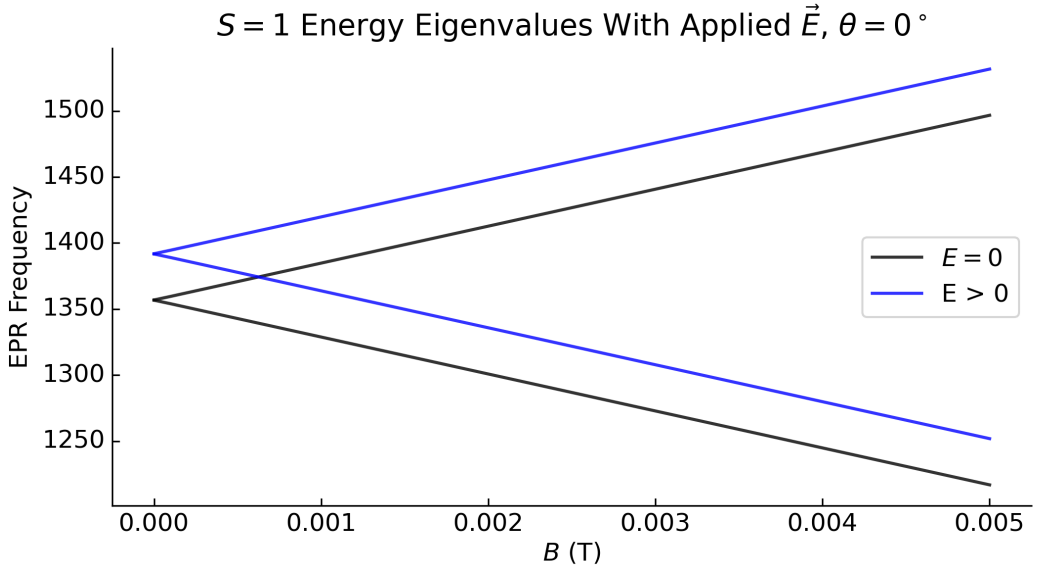

Fig. 2.8: Eigenvalue plot showing...

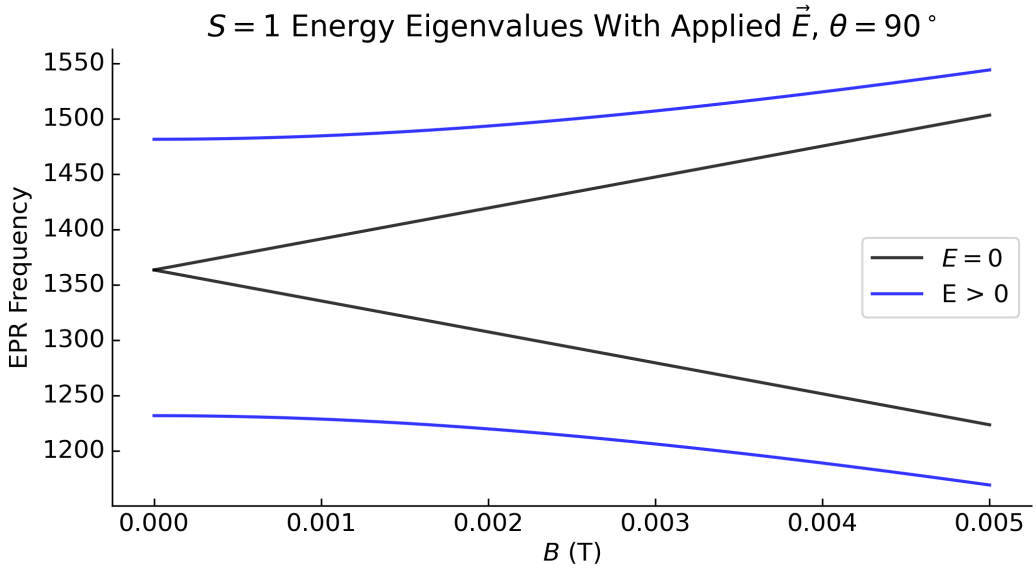

Fig. 2.9: Eigenvalue plot showing...

2.9 Total Hamiltonian

We may therefore consider the total Hamiltonian for our $S = 1, 3/2$ systems as

$$H = H_{\text{Zeeman}} + H_{\text{ZFS}} + H_{\text{Stark}} \tag{2.62}$$

using

$$H_{\text{Zeeman}} = g\mu_B \hat{\vec{S}} \cdot \vec{B}, \tag{2.23}$$

$$H_{\text{ZFS}} = D\left(\hat{S}_z^2 - \frac{1}{3}S(S+1)\right) + E(\hat{S}_x^2 - \hat{S}_y^2), \tag{2.49}$$

and

$$H_{\text{Stark}} = d_{\parallel}E_z\left(\hat{S}_z^2 - \frac{1}{3}S(S+1)\right) - d_{\perp}E_y(\hat{S}_x^2 - \hat{S}_y^2) + d_{\perp}E_x(\hat{S}_x\hat{S}_y + \hat{S}_y\hat{S}_x). \tag{2.61}$$

2.10 Spin Hamiltonian

We can apply (2.62) to our specific $S = 1$ or $S = 3/2$ system by substitution of the spin operators. They are a matrix representation of the $su(2)$ algebra, equivalent to Pauli matrices in the relevant dimension.

2.10.1 $S = 1$ Spin Operators

The three dimensional $S = 1$ spin operators S_j in matrix representation are

$$S_x = \frac{1}{\sqrt{2}} \begin{pmatrix} 0 & 1 & 0 \\ 1 & 0 & 1 \\ 0 & 1 & 0 \end{pmatrix}, S_y = \frac{i}{\sqrt{2}} \begin{pmatrix} 0 & -1 & 0 \\ 1 & 0 & -1 \\ 0 & 1 & 0 \end{pmatrix}, S_z = \frac{1}{\sqrt{2}} \begin{pmatrix} 1 & 0 & 0 \\ 0 & 0 & 0 \\ 0 & 0 & -1 \end{pmatrix}. \tag{2.63}$$

2.10.2 $S = 3/2$ Spin Operators

The four dimensional $S = 3/2$ spin operators S_j in matrix representation are

$$S_x = \frac{1}{2} \begin{pmatrix} 0 & \sqrt{3} & 0 & 0 \\ \sqrt{3} & 0 & 2 & 0 \\ 0 & 2 & 0 & \sqrt{3} \\ 0 & 0 & \sqrt{3} & 0 \end{pmatrix}, \quad S_y = \frac{1}{2i} \begin{pmatrix} 0 & \sqrt{3} & 0 & 0 \\ -\sqrt{3} & 0 & 2 & 0 \\ 0 & -2 & 0 & \sqrt{3} \\ 0 & 0 & -\sqrt{3} & 0 \end{pmatrix},$$
$$S_z = \frac{1}{2} \begin{pmatrix} 3 & 0 & 0 & 0 \\ 0 & 1 & 0 & 0 \\ 0 & 0 & -1 & 0 \\ 0 & 0 & 0 & -3 \end{pmatrix}. \tag{2.64}$$

2.11 Other Factors

2.11.1 Temperature

For SiC divacancies ($S = 1$) the ZFS parameter E shows no dependence on temperature. However, the ZFS parameter D varies with temperature.

D has been measured for both the PL5 and PL6 defects in SiC from close to 0K to around 550K and the dependence of D has been fitted to the change in temperature. Both defects show an approximately linear relationship near room temperature which is shown in Figure 2.10.

More like - v
consider g t
be isotropic
and symmet
ric

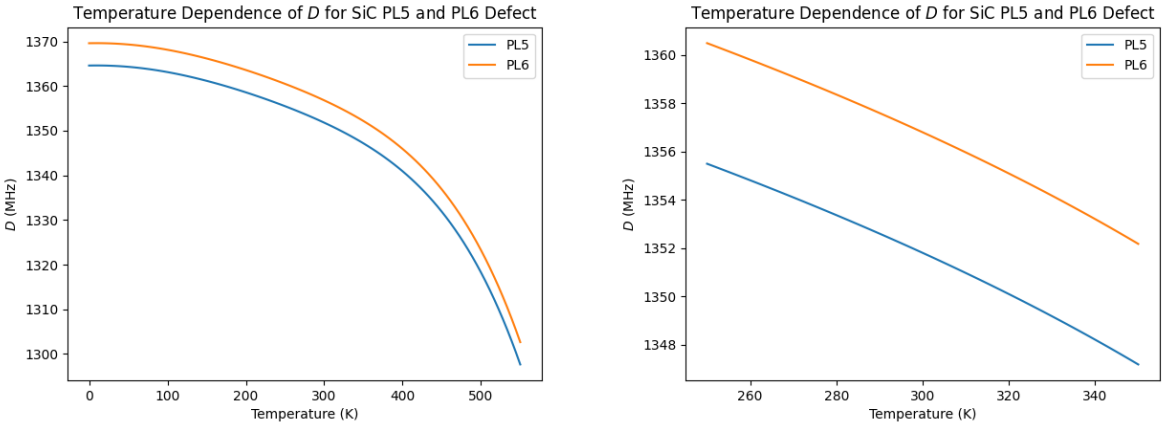

Fig. 2.10: ZFS parameter D temperature dependence for the PL5 and PL6 $S = 1$ defect in SiC from 0-550 K (left) and 250-350 K (right).

tter caption

This allows for the consideration of the system temperature, enabling sensing at a range of temperatures. Additionally, if other parameters are well known, the system may be used as a thermometer.

2.11.2 Strain

Strain, which alters the D and E parameters due to a distribution in the ligand field [35] will influence the Hamiltonian, specifically the zero field splitting of the spin system. Using the same reasoning as in section 2.8, we could derive a strain Hamiltonian which is identical to (2.61). Therefore, exactly as we consider the "whole effect" of the contributions to the zero field Hamiltonian, we consider the combined effect of strain and applied $\vec{E}$. Put simply, strain is treated as an effective electric field [36].

An application of this duality, is that we may use $\vec{E}$ measuring techniques in shielded environment to determine strain.

2.11.3 Pressure

The effect of pressure has been studied for SiC divacancies. The zero field splitting parameter D shows a linear dependence on pressure up to 40 GPa [37] and is shown in figure 2.11.

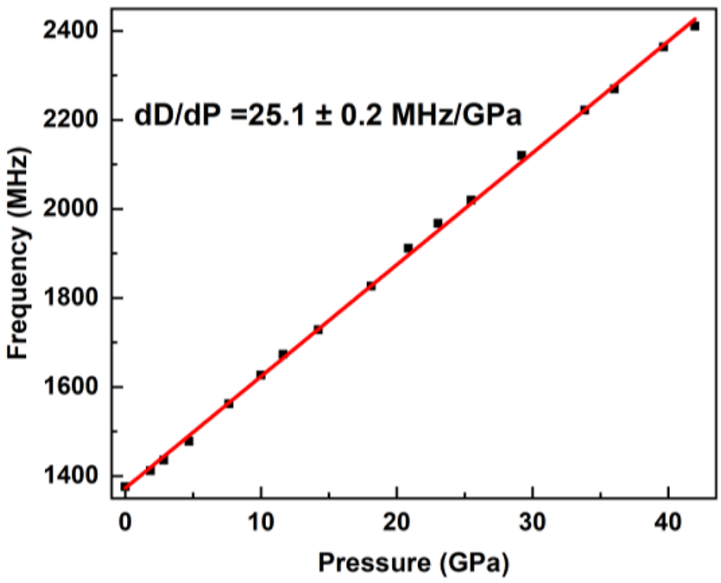

Fig. 2.11: Linear dependence of zero field parameter D to applied pressure as shown in the work by Liu et al.

This allows for the consideration of the pressure applied to the system which allows for sensing in environments above ambient pressure. Additionally, if other parameters are held constant or the sensor is designed such that they cannot contribute (e.g. electro-magnetic shielding) the system can be utilised as a pressure gauge.

Chapter 3

Design

In this chapter we will provide an overview of how the defects in SiC can be used for magnetometry, thermometry and electrometry in isolation. We will then develop a framework where by combining specific defects we may simultaneously measure multiple parameters.

3.1 $S = 1$ Magnetometry

We will consider the use of a SiC divacancy e.g. PL5 or PL6.

We begin with our total Hamiltonian (2.62). We will consider the system under the influence of only the $\vec{B}$ field, so can remove the Stark effect terms. Additionally, for $S = 1$ we may reduce the constant terms [11] leaving

$$H = g\mu_b \hat{\vec{S}} \cdot \vec{B} + D\hat{S}_z^2 + E(\hat{S}_x^2 - \hat{S}_y^2). \tag{3.1}$$

By transforming into spherical coordinates, with θ, ϕ the azimuthal and polar angle respectively and $B = |\vec{B}|$

$$\begin{aligned} B_x &= g\mu_b B \cos\varphi \sin\theta \\ B_y &= g\mu_b B \sin\varphi \sin\theta \\ B_z &= g\mu_b B \cos\theta \end{aligned} \tag{3.2}$$

then substituting the spin operators (2.63) we find

$$H = \begin{pmatrix} D + g\mu_b B \cdot \cos\theta & \frac{g\mu_b B}{\sqrt{2}} \cdot e^{-i\cdot\varphi} \cdot \sin\theta & E \\ \frac{g\mu_b B}{\sqrt{2}} \cdot e^{i\cdot\varphi} \cdot \sin\theta & 0 & \frac{g\mu_b B}{\sqrt{2}} e^{-i\cdot\varphi} \cdot \sin\theta \\ E & \frac{g\mu_b B}{\sqrt{2}} \cdot e^{i\cdot\varphi} \cdot \sin\theta & D - g\mu_b B \cdot \cos\theta \end{pmatrix}. \tag{3.3}$$

3.1.1 $\vec{B}$ Parallel to Defect

It is straightforward to show from (3.3) that if the magnetic field is applied parallel to the defect axis ($\theta = 0$) then the matrix reduces to

$$H = \begin{pmatrix} D + g\mu_b B & 0 & E \\ 0 & 0 & 0 \\ E & 0 & D - g\mu_b B \end{pmatrix}, \tag{3.4}$$

with eigenvalues

$$E_x = E_y = D \pm \sqrt{(g\mu_b B)^2 + E^2},\ E_z = 0. \tag{3.5}$$

The uniaxial symmetry of the SiC divacancy means $D \ll E$. Further, we expect to sense in the range where $g\mu_b B \gg D$ therefore we may write the eigenvalues as

$$E_x = E_y \simeq D \pm g\mu_b B,\ E_z = 0. \tag{3.6}$$

That is, for the transitions between $m_s = 0$ and $m_s = \pm 1$[1], the difference is energy reflected in the EPR spectra (visualised in figure 3.1) is the Zeeman energy

$$\Delta E = g\mu_B B = \gamma B. \tag{2.27}$$

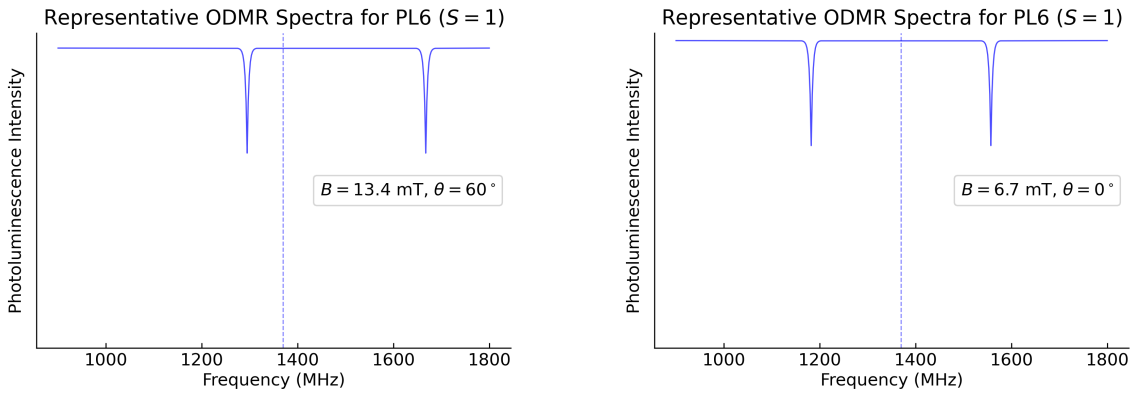

Fig. 3.1: Representative PL6 ODMR spectra showing linear dependence of frequency difference on $B\cos\theta$ and the ZFS shifting of the spectra when $\theta > 0$. Dashed vertical line indicates D.

Thus, for CW-ODMR the difference between the two frequencies $f_1 > f_2$ is directly proportional

[1] These are the allowed transitions for optical depopulation due to selection rules. This may be simply thought of as a helicity conservation as the photon is a $S = 1$ particle.

to B

$$f_1 = D + \gamma B, \quad f_2 = D - \gamma B \tag{3.7}$$

It is then straightforward to calculate B using

$$B = \frac{f_1 - f_2}{2\gamma}. \tag{3.8}$$

3.1.2 Vector Magnetometry

By returning to (3.3) it immediately follows from the characteristic equation that eigenvalues λ satisfy

$$0 = \lambda^3 - 2\lambda^2 D + \frac{D(g\mu_b B)^2}{2} + \lambda(D^2 - E^2 - (g\mu_b B)^2) - \frac{1}{2}(g\mu_b B)^2 \underbrace{\left(D\cos(2\theta) - 2E\cos(2\varphi)\sin^2(\theta)\right)}_{\eta} \tag{3.9}$$

where η depends only on the ZFS parameters and the vector of the applied $\vec{B}$ field.

This allows a more general determination of B from the ODMR spectra using

$$B = \frac{\sqrt{\frac{1}{3}\left(f_1^2 - f_1 f_2 + f_2^2 - D^2 - 3E^2\right)}}{g\mu_B}. \tag{3.10}$$

Further we may find η using

$$\eta = \frac{-7D^3 - 4f_1^3 + 6f_1^2 f_2 + 6f_1 f_2^2 - 4f_2^3 + 3D(9E^2 + f_1^2 - f_1 f_2 + f_2^2)}{9(D^2 + 3E^2 - f_1^2 + f_1 f_2 - f_2^2)}. \tag{3.11}$$

Again, exploiting the uniaxial symmetry of our systems we may reduce our expression for η

$$\eta = D\cos(2\theta) - 2E\cos(2\varphi)\sin^2(\theta) \simeq D\cos 2\theta \tag{3.12}$$

therefore with just two frequencies and knowledge of the ZFS parameters, whilst a complete vector cannot be reconstructed, we may determine the magnitude and azimuthal angle of an applied $\vec{B}$ field

$$\theta = \frac{\cos^{-1}(\eta/D)}{2} \tag{3.13}$$

3.1.3 $S = 1$ Magnetometry Summary

We may achieve angle resolved magnetometry using a $S = 1$ system provided:

1. We can resolve **two frequencies** corresponding to the defect in the CW-ODMR spectra.

2. We know the ZFS parameters D and E.

3. We can determine the magnitude using

$$B = \frac{\sqrt{\frac{1}{3}\left(f_1^2 - f_1 f_2 + f_2^2 - D^2 - 3E^2\right)}}{g\mu_B}. \tag{3.10}$$

4. We can determine the azimuthal angle using

$$\theta = \frac{\cos^{-1}(\eta/D)}{2}. \tag{3.13}$$

3.2 $S = 3/2$ Magnetometry

Now we will consider the use of a SiC Silicon vacancy, specifically V2. For a general $S = 3/2$ system we begin with (2.62). Again we will only consider the influence of the $\vec{B}$ field leaving

$$H = g\mu_b \hat{\vec{S}} \cdot \vec{B} + D\left(\hat{S}_z^2 - \frac{1}{3}S(S+1)\right) + E(\hat{S}_x^2 - \hat{S}_y^2). \tag{3.14}$$

[38] [39] [40]

Distribute refs

If the ZFS interaction of the $S = 3/2$ defect is sufficiently strong, the eigenvalues of the spin Hamiltonian show a strong dependence on the orientation of the applied magnetic field.

This induces a non-linear shift of resonance transitions in EPR frequencies, which is seen in the ODMR spectra. Like $S = 1$, this allows information about the applied external magnetic field to be extracted from EPR spectra provided the ZFS parameters are known.

In zero magnetic field the V_{Si} V2 vacancy has an ODMR line maximum (D) around 70 MHz with very weak dependence on temperature.

In order to reconstruct the energy eigenstates we must use the observed resonant energies. There are $2S + 1$ states for a system with spin S from which $2S$ transition frequencies may be found. Therefore, we may find up to three EPR frequencies.

Using the same polar co-ordinate conversion as (3.2) and $B = |\vec{B}|$ we may write the Hamiltio-

nian in matrix form as

$$H = \begin{pmatrix} D + \frac{3}{2}g\mu_B B \cdot \cos\theta & \frac{\sqrt{3}}{2}g\mu_B B \cdot \sin\theta \cdot e^{-i\varphi} + \sqrt{3}E & 0 & 0 \\ \frac{\sqrt{3}}{2}g\mu_B B \cdot \sin\theta \cdot e^{i\varphi} + \sqrt{3}E & \frac{1}{2}g\mu_B B\cos\theta - D & g\mu_B B \cdot \sin\theta \cdot \cos\varphi + 2E & 0 \\ 0 & g\mu_B B \cdot \sin\theta \cdot \cos\varphi + 2E & -\frac{1}{2}g\mu_B B \cdot \cos\theta - D & \frac{\sqrt{3}}{2}g\mu_B B \cdot \sin\theta \cdot e^{-i\varphi} + \sqrt{3}E \\ 0 & 0 & \frac{\sqrt{3}}{2}g\mu_B B \cdot \sin\theta \cdot e^{i\varphi} + \sqrt{3}E & D - \frac{3}{2}g\mu_B B \cdot \cos\theta \end{pmatrix}. \tag{3.15}$$

3.2.1 $\vec{B}$ Parallel to Defect

Considering B parallel to the defect axis and we find [41] the Hamiltonian reduces to

$$H = \begin{pmatrix} D + \frac{3}{2}g\mu_B B & \sqrt{3}E & 0 & 0 \\ \sqrt{3}E & \frac{1}{2}g\mu_B B - D & 2E & 0 \\ 0 & 2E & -\frac{1}{2}g\mu_B B - D & \sqrt{3}E \\ 0 & 0 & \sqrt{3}E & D - \frac{3}{2}g\mu_B B\cdot \end{pmatrix} \tag{3.16}$$

with eigenvalue equations given by

$$\lambda = \frac{1}{2}g\mu_B B \pm \sqrt{(D + g\mu_B B)^2 + 3E^2} \text{ or, } \lambda = -\frac{1}{2}g\mu_B B \pm \sqrt{(D - g\mu_B B)^2 + 3E^2}. \tag{3.17}$$

Which we further simplify for the Silicon vacancy as $E = 0$ [42] to

$$H = \begin{pmatrix} D + \frac{3}{2}g\mu_B B & 0 & 0 & 0 \\ 0 & \frac{1}{2}g\mu_B B - D & 0 & 0 \\ 0 & 0 & -\frac{1}{2}g\mu_B B - D & 0 \\ 0 & 0 & 0 & D - \frac{3}{2}g\mu_B B \end{pmatrix} \tag{3.18}$$

which is diagonal so we may immediately read off

$$\begin{aligned} \lambda_1 &= \quad 3/2 g\mu_B B + D \\ \lambda_2 &= \quad 1/2 g\mu_B B - D \\ \lambda_3 &= - \quad 1/2 g\mu_B B - D \\ \lambda_4 &= - \quad 3/2 g\mu_B B + D. \end{aligned} \tag{3.19}$$

a sentence to wrap this up

3.2.2 Vector Magnetometry

Coming back to (3.15) we find the eigenvalue equation for a general $S = 3/2$ system to be

$$\begin{aligned}&\lambda^4 - \left(2D^2 + 6E^2 + \frac{5}{2}(g\mu_B B_0)^2\right)\lambda^2 - 2(g\mu_B B_0)^2\left(D(3\cos^2\theta - 1) + 3E\sin^2\theta\cos 2\varphi\right)\lambda \\ &+ \frac{9}{16}(g\mu_B B_0)^4 + D^4 - \frac{1}{2}D^2(g\mu_B B_0)^2 - D^2(g\mu_B B_0)^2(3\cos^2\theta - 1) + 3E^2(3E^2 + 2D^2) \\ &+ E(g\mu_B B_0)^2(6D\sin^2\theta\cos 2\varphi + \frac{9}{2}E\cos 2\theta) = 0.\end{aligned} \tag{3.20}$$

We may write the general equation for the eigenvalues as

$$\sum_{n=0}^{2S+1} C_n \lambda^n = 0 \tag{3.21}$$

we then substitute each eigenvalue λ_i into this general expression to obtain $2S + 1$ equations.

The goal is now to remove all λ_i terms by considering instead the transition frequencies between eigenstates, which are observed in the ODMR spectra. The energy states are not in general sorted with respect to the energy values, so we use the convention that $\lambda_i > \lambda_{i-1}$.

To reduce our number of equations to $2S - 1$ we make the substitutions

$$\lambda_i + \underbrace{\lambda_{i+1} - \lambda_i}_{f_{i+1,i}} = \lambda_{i+1}, \qquad \lambda_i - \underbrace{(\lambda_i - \lambda_{i-1})}_{f_{i,i-1}} = \lambda_{i-1}$$

for each $i = 2, \ldots, 2S$ and calculate both

$$\sum_{n=0}^{2S+1} \frac{C_n\left((\lambda_i + f_{i+1,i})^n - \lambda_i^n\right)}{C_{2S+1}} = 0 \text{ and } \sum_{n=0}^{2S+1} \frac{C_n\left((\lambda_i - f_{i,i-1})^n - \lambda_i^n\right)}{C_{2S+1}} = 0$$

to find two new simultaneous equations

$$\sum_{n=0}^{2S} C'_{i,n}\lambda_i^n = 0 \text{ and } \sum_{n=0}^{2S} C''_{i,n}\lambda_i^n = 0.$$

We may combine these as

$$\sum_{n=0}^{2S} \frac{C'_{i,n}\lambda_i^n}{C'_{i,2S}} - \frac{C''_{i,n}\lambda_i^n}{C''_{i,2S}} = 0$$

to obtain an equation for the eigenvalue of the energy eigenstate $|i\rangle$ where $i = 2, \ldots, 2S$:

$$\sum_{n=0}^{2S-1} C_{i,n}^{(2S-1)}\lambda_i^n = 0. \tag{3.22}$$

This process is repeated until only one linear equation exists for each eigenvalue, which may be expressed in terms of resonant energies. $f_{i,i-1}$ can then be substituted to find expressions for all other eigenvalues. We obtain equations for λ_2 expressed in terms of $f_{2,1}$, $f_{3,2}$ and λ_3 expressed in terms of $f_{3,2}$, $f_{4,3}$.

Finally, using $f_{3,2} = \lambda_3 - \lambda_2$ we find formulas for each eigenvalues in terms of the resonant frequencies:

$$\lambda_1 = -\frac{3}{4}f_{2,1} - \frac{1}{2}f_{3,2} - \frac{1}{4}f_{4,3} \tag{3.23}$$

$$\lambda_2 = \frac{1}{4}f_{2,1} - \frac{1}{2}f_{3,2} - \frac{1}{4}f_{4,3} \tag{3.24}$$

$$\lambda_3 = \frac{1}{4}f_{2,1} + \frac{1}{2}f_{3,2} - \frac{1}{4}f_{4,3} \tag{3.25}$$

$$\lambda_4 = \frac{1}{4}f_{2,1} + \frac{1}{2}f_{3,2} + \frac{1}{4}f_{4,3}. \tag{3.26}$$

We substitute one of these expressions into one of the equations of the form of equation (3.22) and we obtain

$$\begin{aligned} 5(g\mu_B B)^2 = &\left(\frac{\sqrt{3}}{2}f_{4,3} + f_{3,2} + \frac{\sqrt{3}}{2}f_{2,1}\right)^2 \\ &+ (1-\sqrt{3})(f_{4,3}+f_{2,1})f_{3,2} - f_{4,3}f_{2,1} - 4(D^2+3E^2). \end{aligned} \tag{3.27}$$

We also find a $S = 3/2$ η which is again useful for angle resolution as it is dependent on the ZFS parameters, θ and φ

$$\eta \equiv E(2\cos^2\varphi\sin^2\theta + \cos^2\theta) + D\cos^2\theta \tag{3.28}$$

which in terms of the resonant frequencies is given by

$$\eta = \frac{4\left(8(D+3E) + 5(f_{4,3}-f_{2,1})\right)(g\mu_B B)^2 + (f_{4,3}-f_{2,1})\left(16(D^2+3E^2) - (f_{4,3}-f_{2,1})^2 - 4f_{3,2}^2\right)}{96(g\mu_B B)^2} \tag{3.29}$$

where $(g\mu_B B)^2$ may be determined in terms of the frequencies as (3.27).

Overall, this shows that if the ZFS is known and three EPR frequencies are observed, the applied magnetic field strength can be found using (3.27).

Since $E = 0$, $E \ll D$ for the Silicon vacacny, we may approximate η defined in equation (3.28) to

$$\eta \simeq D\cos^2\theta. \tag{3.30}$$

By exploiting this approximation, we can determine the azimuthal angle that the magnetic field vector makes with the defect axis, however at this stage we may not determine anything about the x, y components of the vector.

To do so we explicitly compute η using equation (3.29) then we find the azimuthal angle as

$$\theta = \cos^{-1}\sqrt{\frac{\eta}{D}} \tag{3.31}$$

In a general $S = 3/2$ system, ambiguity is found when computing θ using equation (3.31) as the EPR frequencies can not be mapped to specific transitions.

Finish spin 3/2 magnetometry section, reference using ref B fields and discuss method in paper

.

The following approach exploits the fact that a crossing of resonant frequencies occurs at a given angle (see figure 3.2). The method should be considered for $g\mu_B B_0 \gg 2\sqrt{D^2 + 3E^2}$ explicitly as interactions such as level anti-crossing produce a complex spectra [43] when $g\mu_B B_0 \approx 2\sqrt{D^2 + 3E^2}$ and the invariance of a particular EPR frequency when $g\mu_B B_0 \ll 2\sqrt{D^2 + 3E^2}$ makes determination of the polar angle θ impossible.

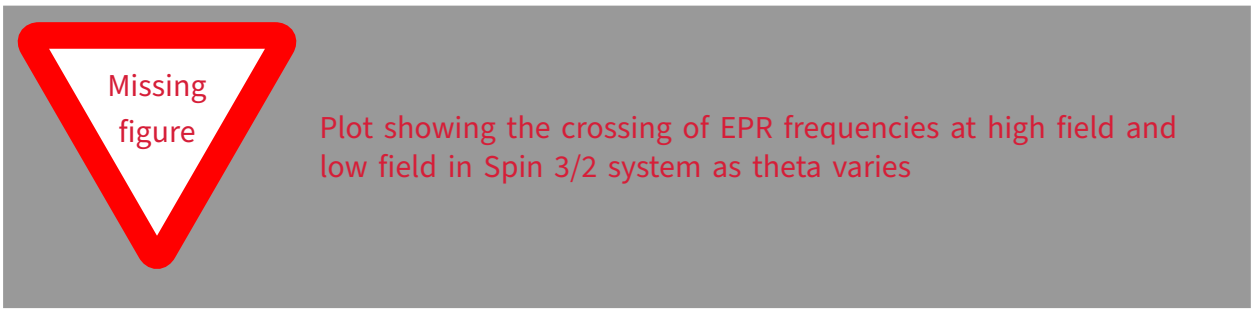

Fig. 3.2:

[44]

3.2.3 $S = 3/2$ Magnetometry Summary

We may achieve angle resolved magnetometry using a $S = 3/2$ system provided:

1. We can resolve **three frequencies** corresponding to the defect in the CW-ODMR spectra.

   add the specific freq we need.

2. We know the ZFS parameters D and E.

3. We can determine the magnitude using

$$5(g\mu_B B)^2 = \left(\frac{\sqrt{3}}{2} f_{4,3} + f_{3,2} + \frac{\sqrt{3}}{2} f_{2,1}\right)^2 + (1-\sqrt{3})(f_{4,3} + f_{2,1}) f_{3,2} - f_{4,3} f_{2,1} - 4(D^2 + 3E^2). \tag{3.27}$$

including the

4. We can determine the azimuthal angle using

$$\theta = \cos^{-1}\sqrt{\frac{\eta}{D}} \tag{3.31}$$

State ambiguity terms

3.3 $S = 1$ Electrometry

Add matrix Hamiltonian as well as eigenval solutions. Include the formula for $\Delta\omega$ and dicuss the diminishing returns when $B \neq 0$ or if $B \not\perp z$

We consider a SiC divacancy and again begin with the total Hamiltonian (2.62). In this case we need all elements of the equation

$$H = g\mu_B \hat{\vec{S}} \cdot \vec{B} + D(\hat{S}_z^2) + E(\hat{S}_x^2 - \hat{S}_y^2) + d_\parallel E_z(\hat{S}_z^2) - d_\perp E_y(\hat{S}_x^2 - \hat{S}_y^2) + d_\perp E_x(\hat{S}_x \hat{S}_y + \hat{S}_y \hat{S}_x). \tag{2.62}$$

For this discussion we will consider the effective electric field as $\vec{\mathcal{E}} = \vec{E} + \vec{\sigma}$ the sum of both the applied field and that which is induced by the strain. Without loss of generality we may switch the x, y which will help in the simplification.

$$H = \begin{pmatrix} D + d_\parallel \mathcal{E}\cos\theta_E + g\mu_b B \cdot \cos\theta_B & \frac{g\mu_b B}{\sqrt{2}} \cdot e^{-i\cdot\varphi_B} \cdot \sin\theta_B & E - d_\perp \mathcal{E} e^{-i\varphi_E}\sin\theta_E \\ \frac{g\mu_b B}{\sqrt{2}} \cdot e^{i\cdot\varphi_B} \cdot \sin\theta_B & 0 & \frac{g\mu_b B}{\sqrt{2}} e^{-i\cdot\varphi_B} \cdot \sin\theta_B \\ E - d_\perp \mathcal{E} e^{i\varphi_E}\sin\theta_E & \frac{g\mu_b B}{\sqrt{2}} \cdot e^{i\cdot\varphi_B} \cdot \sin\theta_B & D + d_\parallel \mathcal{E}\cos\theta_E - g\mu_b B \cdot \cos\theta_B \end{pmatrix}. \tag{3.32}$$

It is easy to see that to maximally reduce the contribution of the magnetic field on the diagonal elements, we should orient the magnetic field perpendicular to the defect ($\theta_B = 90°$). Defining

$\mathcal{E}_\perp = \sqrt{\mathcal{E}_x^2 + \mathcal{E}_y^2}$ and $B_\perp$ similarly, we find if the $\vec{B}$ field was parallel to the defect axis $\theta = 0$ the Hamiltonian reduces to

$$H = \begin{pmatrix} D + d_\parallel \mathcal{E} \cos\theta_E + g\mu_b B & 0 & E - d_\perp \mathcal{E} e^{-i\varphi_E} \sin\theta_E \\ 0 & 0 & 0 \\ E - d_\perp \mathcal{E} e^{i\varphi_E} \sin\theta_E & 0 & D + d_\parallel \mathcal{E} \cos\theta_E - g\mu_b B \end{pmatrix}. \tag{3.33}$$

The eigenvalues may be found as for section 3.1 for the $m_s = 0$ to $m_s = \pm 1$ transitions and are

$$f_\pm \simeq D + d_\parallel \mathcal{E}_\parallel \pm \sqrt{(g\mu_B B)^2 + (d_\perp \mathcal{E}_\perp)^2}. \tag{3.34}$$

Since the parallel component of the field is equivalent to a correction to ZFS D and raises the whole spectra, we find

$$\mathcal{E}_\parallel d_\parallel = \frac{f_1 + f_2}{2} - D. \tag{3.35}$$

We find a similar expression for the perpendicular component as

$$\mathcal{E}_\perp d_\perp = \sqrt{\frac{1}{4}(f_1 - f_2)^2 - (g\mu_B B)^2}. \tag{3.36}$$

Clearly this allows us to deduce the azimuthal angle and magnitude as

$$\theta = \tan^{-1}\left(\frac{\mathcal{E}_\parallel}{\mathcal{E}_\perp}\right), \quad E = \sqrt{\mathcal{E}_\perp^2 + \mathcal{E}_\parallel} \tag{3.37}$$

This method is mathematically sound, but the energy difference is suppressed by the parallel $\vec{B}$ field and would require careful alignment of the magnetic field to the defect axis. A general expression for the difference in EPR frequencies for the $m_s = 0$ to $m_s = \pm 1$, $\Delta f_\pm$ is [45]

$$\Delta f_\pm = d_\parallel E_z \pm \Big(F(\vec{B}, \vec{E}, \vec{\sigma}) - F(\vec{B}, 0, \vec{\sigma})\Big) \tag{3.38}$$

where

$$F(\vec{B}, \vec{E}, \vec{\sigma}) = \left((\mu_B g B_z)^2 + d_\perp^2 \mathcal{E}_\perp^2 - \frac{(\mu_B g B_\perp)^2}{D} d_\perp \mathcal{E}_\perp \cdot \cos(2\varphi_B + \varphi_\mathcal{E}) + \frac{(\mu_B g B_\perp)^4}{4D^2}\right)^{\frac{1}{2}} \tag{3.39}$$

and

$$F(\vec{B}, 0, \vec{\sigma}) = \left((\mu_B g B_z)^2 + d_\perp^2 \sigma_\perp^2 - \frac{(\mu_B g B_\perp)^2}{D} d_\perp \sigma_\perp \cdot \cos(2\varphi_B + \varphi_\sigma) + \frac{(\mu_B g B_\perp)^4}{4D^2}\right)^{\frac{1}{2}}. \tag{3.40}$$

A major benefit of the maturity of SiC manufacturing is that we can produce chips with very little strain, so we may assume that $\vec{\mathcal{E}} = \vec{E}$. This also allows us to reduce the $F(\vec{B}, 0, \vec{\sigma})$ and make

$\Delta f_\pm$ a function only of applied $\vec{B}$ and $\vec{E}$.

If $\vec{B}$ is well known, this reduces to a function of E, θ and ϕ which may be approximated using a best fit algorithm. This means if $\vec{B}$ is well known, then possibilities for $\vec{E}$ can be calculated. This would leave ambiguity in $\vec{E}$ which could be resolved by

Discuss resolving ambiguity

3.3.1 $S = 1$ Electrometry Summary

We may achieve vector electrometry using a triplet state if

1. We can identify three lines.

3.4 $S = 1$ Thermometry

Again for $S = 1$ we will consider a divacancy which have zero- field splitting (ZFS) frequencies are at approximately $D = 1.365$ GHz [46].

For this application we will need every term in (2.62) as D is affected by $\vec{B}$, $\vec{E}$, temperature, and pressure [47]. We will reduce the constant terms as we did in 3.1

$$\begin{aligned} H = {} & g\mu_B \hat{\vec{S}} \cdot \vec{B} + D(\hat{S}_z^2) + E(\hat{S}_x^2 - \hat{S}_y^2) \\ & + d_\parallel E_z(\hat{S}_z^2) - d_\perp E_y(\hat{S}_x^2 - \hat{S}_y^2) + d_\perp E_x(\hat{S}_x\hat{S}_y + \hat{S}_y\hat{S}_x). \end{aligned} \tag{2.62}$$

In this discussion we will consider the pressure to be constant, but as we will describe at the end of this section, by holding temperature constant the same scheme could be used to detect pressure.

There are two main approaches to thermometry:

ZFS Temperature Dependence. The ZFS D may, depending on the specific spin system being studies, be sensitive to changes in temperature, which will be exploited in this section.

Photoluminescence. The photoluminescence of the spin system may have a dependence on temperature, which we will exploit in section 3.5.

We will exploit the temperature dependence of ZFS D which results from thermal lattice expansion and a temperature dependence of the electron–phonon interaction [48, 49]. We will also consider the influences of $\vec{B}$ and $\vec{E}$ to be well known, this could be achieved by careful experiment design or by measurement. We will therefore assume they may be disregarded in this discussion with the exception of a well known $\vec{B}$ field applied along the defect axis.

This allows us to reduce our Hamiltonian down to only

$$H' = D(T)\hat{S}_z^2 \tag{3.41}$$

which when we substitute our spin operator (2.63) we find

$$H' = \begin{pmatrix} D(T) & 0 & 0 \\ 0 & 0 & 0 \\ 0 & 0 & D(T) \end{pmatrix}. \tag{3.42}$$

We see from (3.42) that the $m_s = \pm 1$ states are both uniformly affected by the temperature dependence of D while the $m_s = 0$ state is not influenced by the change. Therefore, the $\Delta m_s = \pm 1$ transitions, detectable in EPR, are affected.

The temperature dependence of D is visualised as a magnetic field is applied along the defect axis in figure 3.3.

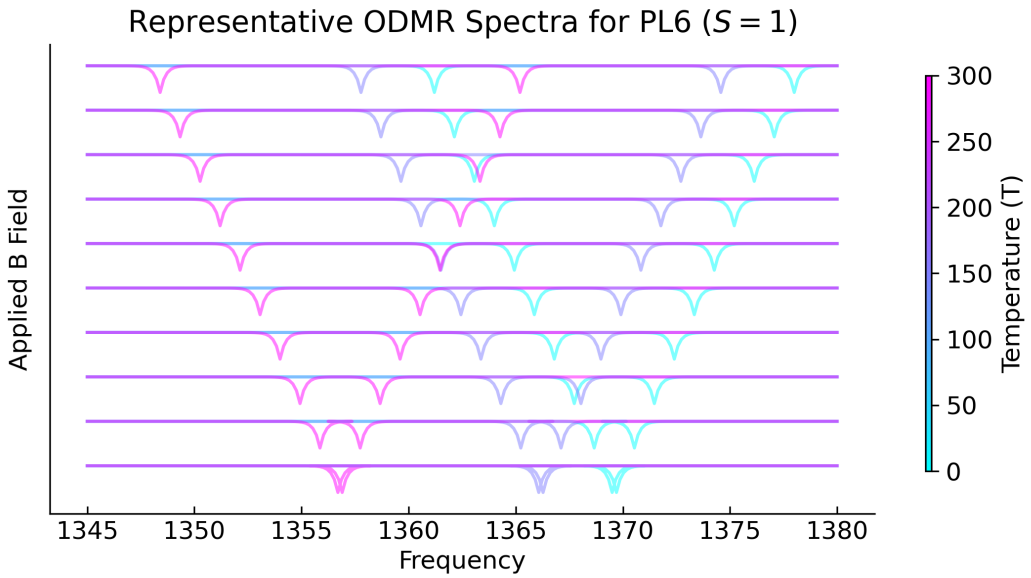

Fig. 3.3

For any $B > 0$, since the Zeeman effect acts on the $m_s = \pm 1$ states symmetrically we may find D using

$$f_1 = D(T) + \gamma B, \quad f_2 = D(T) - \gamma B \tag{3.43}$$

and computing $D(T)$

$$D(T) = \frac{f_1 + f_2}{2}. \tag{3.44}$$

The temperature dependence of D has been studied for both PL5 and PL6 [**?**, **?**]. The PL6 dependence may be fit to the Debye-model formula [50], Varshni-form formula [51] or a polynomial-

form formula [52, 53]

$$D(T) = 1364.6 + 3.5 \times 10^{-3}T - 1.8 \times 10^{-4}T^2 - 1.5 \times 10^{-7}T^3 + 1.6 \times 10^{-9}T^4 - 2.710^{-12}T^5 \text{ MHz}. \tag{3.45}$$

Any of the fits may be used to infer temperature from the measured value of D.

3.4.1 $S = 1$ Thermometry Summary

We may achieve thermometry using a $S = 1$ system provided:

1. The influence of $\vec{B}, \vec{E}$ and pressure are well known.
2. The temperature dependence of the defect has been studied and fit to an equation e.g.

$$D(T) = 1364.6 + 3.5 \times 10^{-3}T - 1.8 \times 10^{-4}T^2 - 1.5 \times 10^{-7}T^3 + 1.6 \times 10^{-9}T^4 - 2.710^{-12}T^5 \text{ MHz}. \tag{3.45}$$

3. We can resolve **one frequency** (in zero field) or **two frequencies** if the $m_s = \pm 1$ degeneracy has been lifted corresponding to the defect in the CW-ODMR spectra. This may be used to find D e.g. with $B \parallel z$ we have

$$D(T) = \frac{f_1 + f_2}{2} \tag{3.44}$$

The methods described in this section have exploited the change of ZFS D due to temperature, which is characteristically the same as the change due to pressure. The scheme may therefore be used for sensing pressure as well as sensing temperature.

3.5 $S = 3/2$ Thermometry

We consider again the V2 Silicon vacancy which due to the 4H-SiC trigonal pyramidal symmetry has a stable ground state ZFS with respect to temperature and can not be used for thermometry [54]. However, the ZFS of the excited state of the Silicon vacancy has a much larger change rate with the temperature compared with the dD/dT of the ground state of the divacancy in 4H-SiC or the NV centre in diamond [55].

Schemas have been developed which exploit the increase in photoluminescence in the vicinity of level anti-crossings

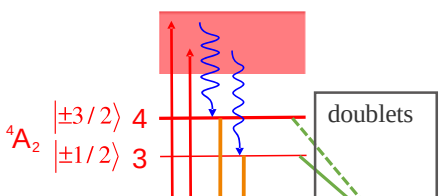

to measure the change in the excited state D as in the work by Anisimov et al.

We will focus instead on an alternative all optical method which exploits the dependence on temperature of the photoluminescence of the spin system.

Anti-Stokes excitation is a process in which the wavelength of the exciting photon is longer (i.e. lower energy) than that of the emitted photons (visualised in figure 3.5). The mechanisms of anti-stokes excitation have been studied and include multiphoton absorption, phonon absorption, and Auger recombination [56, 57].

Since the anti-Stokes excitation process occurs with an energy contribution from the temperature dependent phonons, the ratio between the anti-Stokes and Stokes photoluminescence intensity is proportional to the density of the phonons. The number density of the phonons obeys a Bose–Einstenin distribution [58]

$$\frac{I_{\mathrm{AS}}}{I_{\mathrm{S}}} \propto \exp\left\{\frac{\Delta E}{k_B T} - 1\right\} \tag{3.46}$$

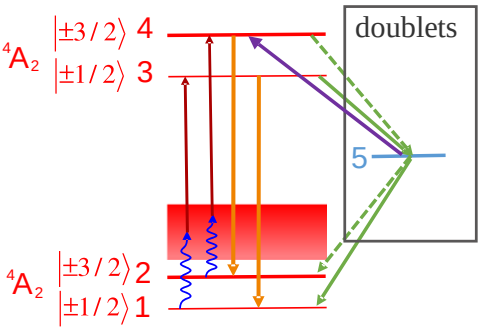

Fig. 3.5: Adapted from Wang et al.

where I_{AS} and I_{S} are the photoluminescence intensities for anti-Stokes and Stokes respectively for a datum laser power. ΔE represents the energy gap between the excitation photon and the zero phonon line i.e. the phonon contribution to the excitation.

We may reduce this to a temperature dependent exponential curve when $\Delta E \ll k_B T$ as (3.46) reduces to

$$\frac{I_{\mathrm{AS}}}{I_{\mathrm{S}}} \propto \exp\left\{\frac{\Delta E}{k_B T}\right\}. \tag{3.47}$$

Wang et al. analysed the anti-Stokes excitation of the Silicon vacancy [1]. The zero phonon line for the defect is around 917nm, so a Stokes excitation was induces by a laser with $1030 > 917$nm and the anti-Stokes excitation was induced by a laser with $720 < 917$nm. Using the same power for both lasers, the intensity of the photoluminescence from the anti-Stokes excitation increased as temperature increased. Conversely the intensity from the Stokes excitation decreased with temperature. The ratio therefore agrees with the statistical model in (3.46).

Thus to realise a thermometer, we fit data to (3.47) with measurable proportionality and correction factors a, b, c, T_0 as [56]

$$\frac{I_{\mathrm{AS}}}{I_{\mathrm{S}}} = a + b \exp\left\{-\frac{c}{T - T_0}\right\}. \tag{3.48}$$

Temperature may then be inferred by solving the equation as

$$T = T_0 - \frac{c}{\ln\left(\left[\frac{I_{\mathrm{AS}}}{I_{\mathrm{S}}} - a\right]/b\right)}. \tag{3.49}$$

For the SiC Silicon vacancy the intensity ratio, and thus the proposed thermometry sensitivity, is most sensitive at room temperature and above.

Affects of other factors? e.g. $\vec{B}, \vec{E}$[1]

3.5.1 $S = 3/2$ Thermometry Summary

We may achieve all optical thermometry using an $S = 3/2$ system provided:

1. We can identify three lines.

Index

Bibliography

[1] Jun-Feng Wang, Fei-Fei Yan, Qiang Li, Zheng-Hao Liu, Jin-Ming Cui, Zhao-Di Liu, Adam Gali, Jin-Shi Xu, Chuan-Feng Li, and Guang-Can Guo. Robust coherent control of solid-state spin qubits using anti-stokes excitation. *Nature Communications*, 12(1), May 2021.

[2] Gabriele Rainò, Nuri Yazdani, Simon C. Boehme, Manuel Kober-Czerny, Chenglian Zhu, Franziska Krieg, Marta D. Rossell, Rolf Erni, Vanessa Wood, Ivan Infante, and Maksym V. Kovalenko. Ultra-narrow room-temperature emission from single cspbbr3 perovskite quantum dots. *Nature Communications*, 13(1), May 2022.

[3] Nguyen T. Son, Christopher P. Anderson, Alexandre Bourassa, Kevin C. Miao, Charles Babin, Matthias Widmann, Matthias Niethammer, Jawad Ul Hassan, Naoya Morioka, Ivan G. Ivanov, Florian Kaiser, Joerg Wrachtrup, and David D. Awschalom. Developing silicon carbide for quantum spintronics. *Applied Physics Letters*, 116(19), May 2020.

[4] David D. Awschalom, Ronald Hanson, Jörg Wrachtrup, and Brian B. Zhou. Quantum technologies with optically interfaced solid-state spins. *Nature Photonics*, 12(9):516–527, August 2018.

[5] Gang Zhang, Yuan Cheng, Jyh-Pin Chou, and Adam Gali. Material platforms for defect qubits and single-photon emitters. *Applied Physics Reviews*, 7(3), September 2020.

[6] Mete Atatüre, Dirk Englund, Nick Vamivakas, Sang-Yun Lee, and Joerg Wrachtrup. Material platforms for spin-based photonic quantum technologies. *Nature Reviews Materials*, 3(5):38–51, April 2018.

[7] Romana Schirhagl, Kevin Chang, Michael Loretz, and Christian L. Degen. Nitrogen-vacancy centers in diamond: Nanoscale sensors for physics and biology. *Annual Review of Physical Chemistry*, 65(1):83–105, April 2014.

[8] B. Hensen, H. Bernien, A. E. Dréau, A. Reiserer, N. Kalb, M. S. Blok, J. Ruitenberg, R. F. L. Vermeulen, R. N. Schouten, C. Abellán, W. Amaya, V. Pruneri, M. W. Mitchell, M. Markham, D. J. Twitchen, D. Elkouss, S. Wehner, T. H. Taminiau, and R. Hanson. Loophole-free bell inequality violation using electron spins separated by 1.3 kilometres. *Nature*, 526(7575):682–686, October 2015.

[9] C. E. Bradley, J. Randall, M. H. Abobeih, R. C. Berrevoets, M. J. Degen, M. A. Bakker, M. Markham, D. J. Twitchen, and T. H. Taminiau. A ten-qubit solid-state spin register with quantum memory up to one minute. *Phys. Rev. X*, 9:031045, Sep 2019.

[10] William F. Koehl, Bob B. Buckley, F. Joseph Heremans, Greg Calusine, and David D. Awschalom. Room temperature coherent control of defect spin qubits in silicon carbide. *Nature*, 479(7371):84–87, November 2011.

[11] David J. Christle, Abram L. Falk, Paolo Andrich, Paul V. Klimov, Jawad Ul Hassan, Nguyen T. Son, Erik Janzén, Takeshi Ohshima, and David D. Awschalom. Isolated electron spins in silicon carbide with millisecond coherence times. *Nature Materials*, 14(2):160–163, December 2014.

[12] Matthias Widmann, Sang-Yun Lee, Torsten Rendler, Nguyen Tien Son, Helmut Fedder, Seoyoung Paik, Li-Ping Yang, Nan Zhao, Sen Yang, Ian Booker, Andrej Denisenko, Mohammad Jamali, S. Ali Momenzadeh, Ilja Gerhardt, Takeshi Ohshima, Adam Gali, Erik Janzén, and J¨ org Wrachtrup. Coherent control of single spins in silicon carbide at room temperature. *Nature Materials*, 14(2):164–168, December 2014.

[13] A. Carrington and A.D. McLachlan. *Introduction to Magnetic Resonance with Applications to Chemistry and Chemical Physics*. A Harper international edition. Harper & Row, 1967.

[14] J. Köhler, J. A. J. M. Disselhorst, M. C. J. M. Donckers, E. J. J. Groenen, J. Schmidt, and W. E. Moerner. Magnetic resonance of a single molecular spin. *Nature*, 363(6426):242–244, May 1993.

[15] Edlyn V. Levine, Matthew J. Turner, Pauli Kehayias, Connor A. Hart, Nicholas Langellier, Raisa Trubko, David R. Glenn, Roger R. Fu, and Ronald L. Walsworth. Principles and techniques of the quantum diamond microscope. *Nanophotonics*, 8(11):1945–1973, 2019.

[16] Lawrence J Berliner and Jacques Reuben, editors. *Spin labeling*. Biological magnetic resonance. Springer, New York, NY, September 2011.

[17] John David Jackson. *Classical Electrodynamics*. John Wiley & Sons, Nashville, TN, 3 edition, July 1998.

[18] David J Griffiths. *Introduction to Electrodynamics*. Pearson, Upper Saddle River, NJ, 4 edition, September 2012.

[19] Bo Chen. *Introduction to NMR*, pages 1–1–1–16. AIP Publishing LLCMelville, New York, October 2020.

[20] D.A. Bromley and W. Greiner. *Quantum Mechanics: An Introduction*. Physics and Astronomy. Springer Berlin Heidelberg, 2000.

[21] Shankar Ramamurti. *Principles of quantum mechanics*. Kluwer Academic/Plenum, Dordrecht, Netherlands, December 1995.

[22] D.C. Giancoli. *Physics for Scientists and Engineers with Modern Physics*. Physics for Scientists & Engineers with Modern Physics. Pearson Education, 2008.

[23] Walther Gerlach and Otto Stern. Das magnetische moment des silberatoms. *Zeitschrift fr Physik*, 9(1):353–355, December 1922.

[24] Bogdan Povh, Klaus Rith, Christoph Scholz, and Frank Zetsche. *Particles and nuclei*. Springer, Berlin, Germany, 3 edition, August 2002.

[25] X. Fan, T. G. Myers, B. A. D. Sukra, and G. Gabrielse. Measurement of the electron magnetic moment. 2022.

[26] X. Fan, T. G. Myers, B. A. D. Sukra, and G. Gabrielse. Measurement of the electron magnetic moment. *Phys. Rev. Lett.*, 130:071801, Feb 2023.

[27] Lucjan Piela. *Singlet and Triplet States for Two Electrons*, page e133–e135. Elsevier, 2014.

[28] V. Nabokov. *THEORETICAL MODELS OF MBE*, page 111–209. Elsevier, 2002.

[29] Jeannine Grüne. *Spin States and Efficiency-Limiting Pathways in Optoelectronic Materials and Devices*. PhD thesis, 2022.

[30] W B Mims. *The linear electric field effect in paramagnetic resonance*. Oxford University Press, London, England, September 1976.

[31] Joel Davidsson, Viktor Ivády, Rickard Armiento, N T Son, Adam Gali, and Igor A Abrikosov. First principles predictions of magneto-optical data for semiconductor point defect identification: the case of divacancy defects in 4h–sic. *New Journal of Physics*, 20(2):023035, February 2018.

[32] Eric Van Oort and Max Glasbeek. Electric-field-induced modulation of spin echoes of n-v centers in diamond. *Chemical Physics Letters*, 168(6):529–532, May 1990.

[33] V. M. Acosta, C. Santori, A. Faraon, Z. Huang, K.-M. C. Fu, A. Stacey, D. A. Simpson, K. Ganesan, S. Tomljenovic-Hanic, A. D. Greentree, S. Prawer, and R. G. Beausoleil. Dynamic stabilization of the optical resonances of single nitrogen-vacancy centers in diamond. *Physical Review Letters*, 108(20), May 2012.

[34] L. C. Bassett, F. J. Heremans, C. G. Yale, B. B. Buckley, and D. D. Awschalom. Electrical tuning of single nitrogen-vacancy center optical transitions enhanced by photoinduced fields. *Physical Review Letters*, 107(26), December 2011.

[35] Gunnar Jeschke. Physical chemistry iv part 2: Electron paramagnetic resonance, 2016.

[36] Abram L. Falk, Paul V. Klimov, Bob B. Buckley, Viktor Ivády, Igor A. Abrikosov, Greg Calusine, William F. Koehl, Ádám Gali, and David D. Awschalom. Electrically and mechanically tunable electron spins in silicon carbide color centers. *Phys. Rev. Lett.*, 112:187601, May 2014.

[37] Lin Liu, Jun-Feng Wang, Xiao-Di Liu, Hai-An Xu, Jin-Ming Cui, Qiang Li, Ji-Yang Zhou, Wu-Xi Lin, Zhen-Xuan He, Wan Xu, Yu Wei, Zheng-Hao Liu, Pu Wang, Zhi-He Hao, Jun-Feng Ding, Hai-Ou Li, Wen Liu, Hao Li, Lixing You, Jin-Shi Xu, Eugene Gregoryanz, Chuan-Feng Li, and Guang-Can Guo. Coherent control and magnetic detection of divacancy spins in silicon carbide at high pressures. *Nano Letters*, 22(24):9943–9950, 2022. PMID: 36507869.

[38] D. Simin, F. Fuchs, H. Kraus, A. Sperlich, P. G. Baranov, G. V. Astakhov, and V. Dyakonov. High-precision angle-resolved magnetometry with uniaxial quantum centers in silicon carbide. *Phys. Rev. Appl.*, 4:014009, Jul 2015.

[39] Sang-Yun Lee, Matthias Niethammer, and Jörg Wrachtrup. Vector magnetometry based on $s = \frac{3}{2}$ electronic spins. *Phys. Rev. B*, 92:115201, Sep 2015.

[40] Sang-Yun Lee, Matthias Niethammer, and Jörg Wrachtrup. Vector magnetometry based on s=3/2 electronic spins. 2015.

[41] Reinhard Kirmse. N. m. atherton. principles of electron spin resonance. ellis horwood and ptr prentice hall, physical chemistry series, ellis horwood, chichester (1993). pp. 585 §127. isbn 0 13 7217625. *Magnetic Resonance in Chemistry*, 33(8):698–698, August 1995.

[42] Roland Nagy, Matthias Niethammer, Matthias Widmann, Yu-Chen Chen, Péter Udvarhelyi, Cristian Bonato, Jawad Ul Hassan, Robin Karhu, Ivan G. Ivanov, Nguyen Tien Son, Jeronimo R. Maze, Takeshi Ohshima, Ö ney O. Soykal, Ádám Gali, Sang-Yun Lee, Florian Kaiser, and Jörg Wrachtrup. High-fidelity spin and optical control of single silicon-vacancy centres in silicon carbide. *Nature Communications*, 10(1), April 2019.

[43] C. L. Degen. Scanning magnetic field microscope with a diamond single-spin sensor. *Applied Physics Letters*, 92(24):243111, June 2008.

[44] J. Isoya, T. Umeda, N. Mizuochi, N. T. Son, E. Janzén, and T. Ohshima. Epr identification of intrinsic defects in sic. *physica status solidi (b)*, 245(7):1298–1314, June 2008.

[45] F. Dolde, H. Fedder, M. W. Doherty, T. Nöbauer, F. Rempp, G. Balasubramanian, T. Wolf, F. Reinhard, L. C. L. Hollenberg, F. Jelezko, and J. Wrachtrup. Electric-field sensing using single diamond spins. *Nature Physics*, 7(6):459–463, April 2011.

[46] Abram L. Falk, Bob B. Buckley, Greg Calusine, William F. Koehl, Viatcheslav V. Dobrovitski, Alberto Politi, Christian A. Zorman, Philip X.-L. Feng, and David D. Awschalom. Polytype control of spin qubits in silicon carbide. *Nature Communications*, 4(1), May 2013.

[47] Masazumi Fujiwara and Yutaka Shikano. Diamond quantum thermometry: from foundations to applications. *Nanotechnology*, 32(48):482002, September 2021.

[48] Viktor Ivády, Tamás Simon, Jeronimo R. Maze, I. A. Abrikosov, and Adam Gali. Pressure and temperature dependence of the zero-field splitting in the ground state of nv centers in diamond: A first-principles study. *Phys. Rev. B*, 90:235205, Dec 2014.

[49] M. W. Doherty, V. M. Acosta, A. Jarmola, M. S. J. Barson, N. B. Manson, D. Budker, and L. C. L. Hollenberg. Temperature shifts of the resonances of the nv^- center in diamond. *Phys. Rev. B*, 90:041201, Jul 2014.

[50] Taras Plakhotnik, Marcus W. Doherty, Jared H. Cole, Robert Chapman, and Neil B. Manson. All-optical thermometry and thermal properties of the optically detected spin resonances of the nv– center in nanodiamond. *Nano Letters*, 14(9):4989–4996, August 2014.

[51] Cong-Cong Li, Ming Gong, Xiang-Dong Chen, Shen Li, Bo-Wen Zhao, Yang Dong, Guang-Can Guo, and Fang-Wen Sun. Temperature dependent energy gap shifts of single color center in diamond based on modified varshni equation. *Diamond and Related Materials*, 74:119–124, April 2017.

[52] Wu-Xi Lin, Fei-Fei Yan, Qiang Li, Jun-feng Wang, Zhi-He Hao, Ji-Yang Zhou, Hao Li, Li-Xing You, Jin-Shi Xu, Chuan-Feng Li, and Guang-Can Guo. Temperature dependence of divacancy spin coherence in implanted silicon carbide. *Phys. Rev. B*, 104:125305, Sep 2021.

[53] Fei-Fei Yan, Jun-Feng Wang, Qiang Li, Ze-Di Cheng, Jin-Ming Cui, Wen-Zheng Liu, Jin-Shi Xu, Chuan-Feng Li, and Guang-Can Guo. Coherent control of defect spins in silicon carbide above 550 k. *Physical Review Applied*, 10(4), October 2018.

[54] S Castelletto, C T-K Lew, Wu-Xi Lin, and Jin-Shi Xu. Quantum systems in silicon carbide for sensing applications. *Reports on Progress in Physics*, 87(1):014501, dec 2023.

[55] A. N. Anisimov, D. Simin, V. A. Soltamov, S. P. Lebedev, P. G. Baranov, G. V. Astakhov, and V. Dyakonov. Optical thermometry based on level anticrossing in silicon carbide. *Scientific Reports*, 6(1), September 2016.

[56] Toan Trong Tran, Blake Regan, Evgeny A. Ekimov, Zhao Mu, Yu Zhou, Wei-bo Gao, Prineha Narang, Alexander S. Solntsev, Milos Toth, Igor Aharonovich, and Carlo Bradac. Anti-stokes excitation of solid-state quantum emitters for nanoscale thermometry. *Science Advances*, 5(5), May 2019.

[57] Jun-Feng Wang, Qiang Li, Fei-Fei Yan, He Liu, Guo-Ping Guo, Wei-Ping Zhang, Xiong Zhou, Li-Ping Guo, Zhi-Hai Lin, Jin-Ming Cui, Xiao-Ye Xu, Jin-Shi Xu, Chuan-Feng Li, and Guang-Can Guo. On-demand generation of single silicon vacancy defects in silicon carbide. *ACS Photonics*, 6(7):1736–1743, May 2019.

[58] Qixing Wang, Qi Zhang, Xiaoxu Zhao, Xin Luo, Calvin Pei Yu Wong, Junyong Wang, Dongyang Wan, T. Venkatesan, Stephen J. Pennycook, Kian Ping Loh, Goki Eda, and Andrew T. S. Wee. Photoluminescence upconversion by defects in hexagonal boron nitride. *Nano Letters*, 18(11):6898–6905, 2018. PMID: 30260651.

[59] C. L. Degen, F. Reinhard, and P. Cappellaro. Quantum sensing. *Rev. Mod. Phys.*, 89:035002, Jul 2017.

[60] John F. Barry, Jennifer M. Schloss, Erik Bauch, Matthew J. Turner, Connor A. Hart, Linh M. Pham, and Ronald L. Walsworth. Sensitivity optimization for nv-diamond magnetometry. *Rev. Mod. Phys.*, 92:015004, Mar 2020.

[61] V. A. Soltamov, C. Kasper, A. V. Poshakinskiy, A. N. Anisimov, E. N. Mokhov, A. Sperlich, S. A. Tarasenko, P. G. Baranov, G. V. Astakhov, and V. Dyakonov. Excitation and coherent control of spin qudit modes in silicon carbide at room temperature. *Nature Communications*, 10(1), April 2019.

[62] Carmem M Gilardoni, Tom Bosma, Danny van Hien, Freddie Hendriks, Björn Magnusson, Alexandre Ellison, Ivan G Ivanov, N T Son, and Caspar H van der Wal. Spin-relaxation times exceeding seconds for color centers with strong spin–orbit coupling in sic. *New Journal of Physics*, 22(10):103051, October 2020.

[63] Oscar Bulancea-Lindvall, Nguyen T. Son, Igor A. Abrikosov, and Viktor Ivády. Dipolar spin relaxation of divacancy qubits in silicon carbide. *npj Computational Materials*, 7(1), December 2021.

[64] T. Astner, P. Koller, C. M. Gilardoni, J. Hendriks, N. T. Son, I. G. Ivanov, J. U. Hassan, C. H. van der Wal, and M. Trupke. Vanadium in silicon carbide: Telecom-ready spin centres with long relaxation lifetimes and hyperfine-resolved optical transitions, 2022.

[65] F. Fuchs, B. Stender, M. Trupke, D. Simin, J. Pflaum, V. Dyakonov, and G. V. Astakhov. Engineering near-infrared single-photon emitters with optically active spins in ultrapure silicon carbide. *Nature Communications*, 6(1), July 2015.

[66] Yiu Yung Pang Wai Kuen Leung Nan Zhao Kin On Ho, Yang Shen and Sen Yang. Diamond quantum sensors: from physics to applications on condensed matter research. *Functional Diamond*, 1(1):160–173, 2021.

[67] Yuzhou Wu, Fedor Jelezko, Martin B Plenio, and Tanja Weil. Diamond quantum devices in biology. *Angewandte Chemie International Edition*, 55(23):6586–6598, April 2016.

[68] Scott E. Crawford, Roman A. Shugayev, Hari P. Paudel, Ping Lu, Madhava Syamlal, Paul R. Ohodnicki, Benjamin Chorpening, Randall Gentry, and Yuhua Duan. Quantum sensing

for energy applications: Review and perspective. *Advanced Quantum Technologies*, 4(8), June 2021.

[69] C. R. Eddy and D. K. Gaskill. Silicon carbide as a platform for power electronics. *Science*, 324(5933):1398–1400, June 2009.

[70] J.B. Casady and R.W. Johnson. Status of silicon carbide (sic) as a wide-bandgap semiconductor for high-temperature applications: A review. *Solid-State Electronics*, 39(10):1409–1422, 1996.

[71] Gary Wolfowicz, F. Joseph Heremans, Christopher P. Anderson, Shun Kanai, Hosung Seo, Adam Gali, Giulia Galli, and David D. Awschalom. Quantum guidelines for solid-state spin defects. *Nature Reviews Materials*, 6(10):906–925, April 2021.

[72] Jun-Feng Wang, Jin-Ming Cui, Fei-Fei Yan, Qiang Li, Ze-Di Cheng, Zheng-Hao Liu, Zhi-Hai Lin, Jin-Shi Xu, Chuan-Feng Li, and Guang-Can Guo. Optimization of power broadening in optically detected magnetic resonance of defect spins in silicon carbide. *Phys. Rev. B*, 101:064102, Feb 2020.

[73] Qiang Li, Jun-Feng Wang, Fei-Fei Yan, Ji-Yang Zhou, Han-Feng Wang, He Liu, Li-Ping Guo, Xiong Zhou, Adam Gali, Zheng-Hao Liu, Zu-Qing Wang, Kai Sun, Guo-Ping Guo, Jian-Shun Tang, Hao Li, Li-Xing You, Jin-Shi Xu, Chuan-Feng Li, and Guang-Can Guo. Room-temperature coherent manipulation of single-spin qubits in silicon carbide with a high readout contrast. *National Science Review*, 9(5):nwab122, 07 2021.

[74] A. V. Poshakinskiy and G. V. Astakhov. Optically detected spin-mechanical resonance in silicon carbide membranes. *Phys. Rev. B*, 100:094104, Sep 2019.

[75] Gary Wolfowicz, Christopher P. Anderson, Andrew L. Yeats, Samuel J. Whiteley, Jens Niklas, Oleg G. Poluektov, F. Joseph Heremans, and David D. Awschalom. Optical charge state control of spin defects in 4h-sic. *Nature Communications*, 8(1), November 2017.

[76] Nguyen T. Son and Ivan G. Ivanov. Charge state control of the silicon vacancy and divacancy in silicon carbide. *Journal of Applied Physics*, 129(21), June 2021.

[77] A. Csóré, I. G. Ivanov, N. T. Son, and A. Gali. Fluorescence spectrum and charge state control of divacancy qubits via illumination at elevated temperatures in $4h$ silicon carbide. *Phys. Rev. B*, 105:165108, Apr 2022.

[78] Christopher P Anderson, Elena O Glen, Cyrus Zeledon, Alexandre Bourassa, Yu Jin, Yizhi Zhu, Christian Vorwerk, Alexander L Crook, Hiroshi Abe, Jawad Ul-Hassan, Takeshi Ohshima, Nguyen T Son, Giulia Galli, and David D Awschalom. Five-second coherence of a single spin with single-shot readout in silicon carbide. *Sci. Adv.*, 8(5):eabm5912, February 2022.

[79] Corey J. Cochrane, Jordana Blacksberg, Mark A. Anders, and Patrick M. Lenahan. Vectorized magnetometer for space applications using electrical readout of atomic scale defects in silicon carbide. *Scientific Reports*, 6(1), November 2016.

[80] Matthias Niethammer, Matthias Widmann, Torsten Rendler, Naoya Morioka, Yu-Chen Chen, Rainer Stöhr, Jawad Ul Hassan, Shinobu Onoda, Takeshi Ohshima, Sang-Yun Lee, Amlan Mukherjee, Junichi Isoya, Nguyen Tien Son, and Jörg Wrachtrup. Coherent electrical readout of defect spins in silicon carbide by photo-ionization at ambient conditions. *Nature Communications*, 10(1), December 2019.

[81] H. Kraus, V. A. Soltamov, F. Fuchs, D. Simin, A. Sperlich, P. G. Baranov, G. V. Astakhov, and V. Dyakonov. Magnetic field and temperature sensing with atomic-scale spin defects in silicon carbide. *Scientific Reports*, 4(1), July 2014.

[82] Matthias Niethammer, Matthias Widmann, Sang-Yun Lee, Pontus Stenberg, Olof Kordina, Takeshi Ohshima, Nguyen Tien Son, Erik Janzén, and Jörg Wrachtrup. Vector magnetometry using silicon vacancies in $4h$-sic under ambient conditions. *Phys. Rev. Appl.*, 6:034001, Sep 2016.

[83] John B. S. Abraham, Cameron Gutgsell, Dalibor Todorovski, Scott Sperling, Jacob E. Epstein, Brian S. Tien-Street, Timothy M. Sweeney, Jeremiah J. Wathen, Elizabeth A. Pogue, Peter G. Brereton, Tyrel M. McQueen, Wesley Frey, B. D. Clader, and Robert Osiander. Nanotesla magnetometry with the silicon vacancy in silicon carbide. *Phys. Rev. Appl.*, 15:064022, Jun 2021.

[84] Lin Liu, Jun-Feng Wang, Xiao-Di Liu, Hai-An Xu, Jin-Ming Cui, Qiang Li, Ji-Yang Zhou, Wu-Xi Lin, Zhen-Xuan He, Wan Xu, Yu Wei, Zheng-Hao Liu, Pu Wang, Zhi-He Hao, Jun-Feng Ding, Hai-Ou Li, Wen Liu, Hao Li, Lixing You, Jin-Shi Xu, Eugene Gregoryanz, Chuan-Feng Li, and Guang-Can Guo. Coherent control and magnetic detection of divacancy spins in silicon carbide at high pressures. *Nano Letters*, 22(24):9943–9950, December 2022.

[85] Zhengzhi Jiang, Hongbing Cai, Robert Cernansky, Xiaogang Liu, and Weibo Gao. Quantum sensing of radio-frequency signal with nv centers in sic. *Science Advances*, 9(20), May 2023.

[86] Yu Zhou, Junfeng Wang, Xiaoming Zhang, Ke Li, Jianming Cai, and Weibo Gao. Self-protected thermometry with infrared photons and defect spins in silicon carbide. *Phys. Rev. Appl.*, 8:044015, Oct 2017.

[87] Takeshi Ohshima, Takahiro Satoh, Hannes Kraus, Georgy V Astakhov, Vladimir Dyakonov, and Pavel G Baranov. Creation of silicon vacancy in silicon carbide by proton beam writing toward quantum sensing applications. *Journal of Physics D: Applied Physics*, 51(33):333002, July 2018.

[88] G. Wolfowicz, S. J. Whiteley, and D. D. Awschalom. Electrometry by optical charge conversion of deep defects in 4h-sic. *Proceedings of the National Academy of Sciences*, 115(31):7879–7883, July 2018.

[89] Stefania Castelletto, Alberto Peruzzo, Cristian Bonato, Brett C. Johnson, Marina Radulaski, Haiyan Ou, Florian Kaiser, and Joerg Wrachtrup. Silicon carbide photonics bridging quantum technology. *ACS Photonics*, 9(5):1434–1457, April 2022.

[90] Shun Kanai, F. Joseph Heremans, Hosung Seo, Gary Wolfowicz, Christopher P. Anderson, Sean E. Sullivan, Mykyta Onizhuk, Giulia Galli, David D. Awschalom, and Hideo Ohno. Generalized scaling of spin qubit coherence in over 12, 000 host materials. *Proceedings of the National Academy of Sciences*, 119(15), April 2022.

[91] Ilja Fescenko, Andrey Jarmola, Igor Savukov, Pauli Kehayias, Janis Smits, Joshua Damron, Nathaniel Ristoff, Nazanin Mosavian, and Victor M. Acosta. Diamond magnetometer enhanced by ferrite flux concentrators. *Phys. Rev. Res.*, 2:023394, Jun 2020.

[92] Tianyu Xie, Zhiyuan Zhao, Xi Kong, Wenchao Ma, Mengqi Wang, Xiangyu Ye, Pei Yu, Zhiping Yang, Shaoyi Xu, Pengfei Wang, Ya Wang, Fazhan Shi, and Jiangfeng Du. Beating the standard quantum limit under ambient conditions with solid-state spins. *Science Advances*, 7(32), August 2021.

[93] Stefania Castelletto and Alberto Boretti. Silicon carbide color centers for quantum applications. *JPhys Photonics*, 2(2):022001, April 2020.

[94] Ö. O. Soykal, Pratibha Dev, and Sophia E. Economou. Silicon vacancy center in $4h$-sic: Electronic structure and spin-photon interfaces. *Phys. Rev. B*, 93:081207, Feb 2016.

[95] S. A. Tarasenko, A. V. Poshakinskiy, D. Simin, V. A. Soltamov, E. N. Mokhov, P. G. Baranov, V. Dyakonov, and G. V. Astakhov. Spin and optical properties of silicon vacancies in silicon carbide a review. *physica status solidi (b)*, 255(1), September 2017.

[96] Fei-Fei Yan, Ai-Lun Yi, Jun-Feng Wang, Qiang Li, Pei Yu, Jia-Xiang Zhang, Adam Gali, Ya Wang, Jin-Shi Xu, Xin Ou, Chuan-Feng Li, and Guang-Can Guo. Room-temperature coherent control of implanted defect spins in silicon carbide. *npj Quantum Information*, 6(1), May 2020.

[97] H. Kraus, V. A. Soltamov, D. Riedel, S. Väth, F. Fuchs, A. Sperlich, P. G. Baranov, V. Dyakonov, and G. V. Astakhov. Room-temperature quantum microwave emitters based on spin defects in silicon carbide. *Nature Physics*, 10(2):157–162, December 2013.

[98] Zhao Mu, Soroush Abbasi Zargaleh, Hans J¨ urgen von Bardeleben, Johannes E. Fröch, Milad Nonahal, Hongbing Cai, Xinge Yang, Jianqun Yang, Xingji Li, Igor Aharonovich, and Weibo Gao. Coherent manipulation with resonant excitation and single emitter creation

of nitrogen vacancy centers in 4h silicon carbide. *Nano Letters*, 20(8):6142–6147, July 2020.

[99] Jun-Feng Wang, Fei-Fei Yan, Qiang Li, Zheng-Hao Liu, He Liu, Guo-Ping Guo, Li-Ping Guo, Xiong Zhou, Jin-Ming Cui, Jian Wang, Zong-Quan Zhou, Xiao-Ye Xu, Jin-Shi Xu, Chuan-Feng Li, and Guang-Can Guo. Coherent control of nitrogen-vacancy center spins in silicon carbide at room temperature. *Phys. Rev. Lett.*, 124:223601, Jun 2020.

[100] Hosung Seo, Abram L Falk, Paul V Klimov, Kevin C Miao, Giulia Galli, and David D Awschalom. Quantum decoherence dynamics of divacancy spins in silicon carbide. *Nat. Commun.*, 7(1):12935, September 2016.

[101] Fei-Fei Yan, Jun-Feng Wang, Qiang Li, Ze-Di Cheng, Jin-Ming Cui, Wen-Zheng Liu, Jin-Shi Xu, Chuan-Feng Li, and Guang-Can Guo. Coherent control of defect spins in silicon carbide above 550 k. *Phys. Rev. Appl.*, 10:044042, Oct 2018.

[102] Qin-Yue Luo, Shuang Zhao, Qi-Cheng Hu, Wei-Ke Quan, Zi-Qi Zhu, Jia-Jun Li, and Jun-Feng Wang. High-sensitivity silicon carbide divacancy-based temperature sensing. *Nanoscale*, 15:8432–8436, 2023.

[103] Andrea Morello, Jarryd J. Pla, Floris A. Zwanenburg, Kok W. Chan, Kuan Y. Tan, Hans Huebl, Mikko Möttönen, Christopher D. Nugroho, Changyi Yang, Jessica A. van Donkelaar, Andrew D. C. Alves, David N. Jamieson, Christopher C. Escott, Lloyd C. L. Hollenberg, Robert G. Clark, and Andrew S. Dzurak. Single-shot readout of an electron spin in silicon. *Nature*, 467(7316):687–691, September 2010.

[104] Yu-Wei Liao, Qiang Li, Mu Yang, Zheng-Hao Liu, Fei-Fei Yan, Jun-Feng Wang, Ji-Yang Zhou, Wu-Xi Lin, Yi-Dan Tang, Jin-Shi Xu, Chuan-Feng Li, and Guang-Can Guo. Deep-learning-enhanced single-spin readout in silicon carbide at room temperature. *Phys. Rev. Appl.*, 17:034046, Mar 2022.

[105] Junfeng Wang, Fupan Feng, Jian Zhang, Jihong Chen, Zhongcheng Zheng, Liping Guo, Wenlong Zhang, Xuerui Song, Guoping Guo, Lele Fan, Chongwen Zou, Liren Lou, Wei Zhu, and Guanzhong Wang. High-sensitivity temperature sensing using an implanted single nitrogen-vacancy center array in diamond. *Phys. Rev. B*, 91:155404, Apr 2015.

[106] Wei-Ke Quan, Lin Liu, Qin-Yue Luo, Xiao-Di Liu, and Jun-Feng Wang. Fiber-coupled silicon carbide divacancy magnetometer and thermometer. *Opt. Express*, 31(10):15592–15598, May 2023.

[107] P. V. Klimov, A. L. Falk, B. B. Buckley, and D. D. Awschalom. Electrically driven spin resonance in silicon carbide color centers. *Phys. Rev. Lett.*, 112:087601, Feb 2014.

[108] Stefania Castelletto, Abdul Salam Al Atem, Faraz Ahmed Inam, Hans Jürgen von Bardeleben, Sophie Hameau, Ahmed Fahad Almutairi, Gérard Guillot, Shin-ichiro Sato, Alberto Boretti, and Jean Marie Bluet. Deterministic placement of ultra-bright near-infrared color centers in arrays of silicon carbide micropillars. *Beilstein Journal of Nanotechnology*, 10:2383–2395, December 2019.

[109] F. Sardi, T. Kornher, M. Widmann, R. Kolesov, F. Schiller, T. Reindl, M. Hagel, and J. Wrachtrup. Scalable production of solid-immersion lenses for quantum emitters in silicon carbide. *Applied Physics Letters*, 117(2), July 2020.

[110] Erik R. Eisenach, John F. Barry, Michael F. O'Keeffe, Jennifer M. Schloss, Matthew H. Steinecker, Dirk R. Englund, and Danielle A. Braje. Cavity-enhanced microwave readout of a solid-state spin sensor. *Nature Communications*, 12(1), March 2021.

[111] Ji-Yang Zhou, Qiang Li, Zhi-He Hao, Wu-Xi Lin, Zhen-Xuan He, Rui-Jian Liang, Liping Guo, Hao Li, Lixing You, Jian-Shun Tang, Jin-Shi Xu, Chuan-Feng Li, and Guang-Can Guo. Plasmonic-enhanced bright single spin defects in silicon carbide membranes. *Nano Letters*, 23(10):4334–4343, May 2023.

[112] Gopalakrishnan Balasubramanian, Philipp Neumann, Daniel Twitchen, Matthew Markham, Roman Kolesov, Norikazu Mizuochi, Junichi Isoya, Jocelyn Achard, Johannes Beck, Julia Tissler, Vincent Jacques, Philip R. Hemmer, Fedor Jelezko, and Jörg Wrachtrup. Ultralong spin coherence time in isotopically engineered diamond. *Nature Materials*, 8(5):383–387, April 2009.

[113] David P. DiVincenzo. Quantum computation. *Science*, 270(5234):255–261, October 1995.

[114] Johann-Martin Spaeth, Jürgen R. Niklas, and Ralph H. Bartram. *Structural Analysis of Point Defects in Solids*. Springer Berlin Heidelberg, 1992.

[115] Johann-Martin Spaeth and Harald Overhof. *Point Defects in Semiconductors and Insulators: Determination of Atomic and Electronic Structure from Paramagnetic Hyperfine Interactions*. Springer Berlin Heidelberg, 2003.

[116] John A. Weil and James R. Bolton. *Electron Paramagnetic Resonance: Elementary Theory and Practical Applications*. Wiley, May 2006.

[117] J. Wrachtrup, C. von Borczyskowski, J. Bernard, M. Orrit, and R. Brown. Optical detection of magnetic resonance in a single molecule. *Nature*, 363(6426):244–245, May 1993.

[118] X.-D. Chen, C.-H. Dong, F.-W. Sun, C.-L. Zou, J.-M. Cui, Z.-F. Han, and G.-C. Guo. Temperature dependent energy level shifts of nitrogen-vacancy centers in diamond. *Applied Physics Letters*, 99(16), October 2011.

[119] P Ščajev and K Jarašiūnas. Application of a time-resolved four-wave mixing technique for the determination of thermal properties of 4h–sic crystals. *Journal of Physics D: Applied Physics*, 42(5):055413, February 2009.

[120] Toeno van der Sar. Magnetometry with spins in diamond. Measuring a magnetic field with NV spins. Measuring a magnetic field with NV spins - Magnetometry with spins in diamond. (n.d.). https://magnetometryrp.quantumtinkerer.tudelft.nl/3_NVspin/. [Accessed 05-08-2024].

[121] Linh Pham, Nir Bar-Gill, David Le Sage, A. Stacey, M. Markham, Daniel Twitchen, M. Lukin, and R. Walsworth. Enhanced metrology using preferential orientation of nitrogen-vacancy centers in diamond. *Physical Review B*, 86, 07 2012.

[122] Gopalakrishnan Balasubramanian, I. Y. Chan, Roman Kolesov, Mohannad Al-Hmoud, Julia Tisler, Chang Shin, Changdong Kim, Aleksander Wojcik, Philip R. Hemmer, Anke Krueger, Tobias Hanke, Alfred Leitenstorfer, Rudolf Bratschitsch, Fedor Jelezko, and Jörg Wrachtrup. Nanoscale imaging magnetometry with diamond spins under ambient conditions. *Nature*, 455(7213):648–651, October 2008.

[123] Erik Janzén, Adam Gali, Patrick Carlsson, Andreas Gällstr öm, Björn Magnusson, and N.T. Son. The silicon vacancy in sic. *Physica B: Condensed Matter*, 404(22):4354–4358, December 2009.

[124] A. Lohrmann, N. Iwamoto, Z. Bodrog, S. Castelletto, T. Ohshima, T. J. Karle, A. Gali, S. Prawer, J. C. McCallum, and B. C. Johnson. Single-photon emitting diode in silicon carbide. 2015.

[125] Pavel Baranov Baranov, Hans Jurgen Von Bardeleben, Fedor Jelezko, and Jorg Wrachtrup. *Magnetic resonance of semiconductors and their nanostructures*. Springer series in materials science. Springer, Vienna, Austria, 1 edition, March 2017.

[126] Peter W Atkins and Ronald S Friedman. *Molecular Quantum Mechanics*. Oxford University Press, London, England, 5 edition, November 2010.

[127] P. V. Klimov, A. L. Falk, B. B. Buckley, and D. D. Awschalom. Electrically driven spin resonance in silicon carbide color centers. *Physical Review Letters*, 112(8), February 2014.

[128] Felix M. Stürner, Andreas Brenneis, Thomas Buck, Julian Kassel, Robert Rölver, Tino Fuchs, Anton Savitsky, Dieter Suter, Jens Grimmel, Stefan Hengesbach, Michael Förtsch, Kazuo Nakamura, Hitoshi Sumiya, Shinobu Onoda, Junichi Isoya, and Fedor Jelezko. Integrated and portable magnetometer based on nitrogen-vacancy ensembles in diamond. *Advanced Quantum Technologies*, 4(4), February 2021.

[129] *Electron Paramagnetic Resonance: A Practitioner's Toolkit*. Wiley, July 2008.

[130] Daniella Goldfarb and Stefan Stoll, editors. *EPR spectroscopy*. eMagRes Books. Standards Information Network, March 2018.

[131] Sabine Richert, Claudia E. Tait, and Christiane R. Timmel. Delocalisation of photoexcited triplet states probed by transient epr and hyperfine spectroscopy. *Journal of Magnetic Resonance*, 280:103–116, July 2017.

[132] Qin-Yue Luo, Shuang Zhao, Qi-Cheng Hu, Wei-Ke Quan, Zi-Qi Zhu, Jia-Jun Li, and Jun-Feng Wang. High sensitivity silicon carbide divacancy-based thermometer, 2023.

[133] M. S. J Barson, L. M. Oberg, L. P. McGuinness, A. Denisenko, N. B. Manson, J. Wrachtrup, and M. W. Doherty. Nanoscale vector electric field imaging using a single electron spin. 2020.